INSTITUTE OF PHYSICS PUBLISHING JOURNAL OF PHYSICS: CONDENSED MATTER

J. Phys.: Condens. Matter **18** (2006) S2595–S2621 doi:10.1088/0953-8984/18/38/S05

Langevin dynamic simulations of fast remagnetization processes in ferrofluids with internal magnetic degrees of freedom

D V Berkov[1], **N L Gorn**[1], **R Schmitz**[2] **and D Stock**[1]

[1] Innovent Technology Development, Pruessingstraße 27B, D-07745 Jena, Germany
[2] Institute of Theoretical Physics C, RWTH Aachen, 52056 Aachen, Germany

Received 5 May 2006, in final form 13 July 2006
Published 8 September 2006
Online at stacks.iop.org/JPhysCM/18/S2595

Abstract

In this paper we present a model which allows numerical studies of ferrofluid dynamics taking into account the internal magnetic degrees of freedom of the ferrofluid particles. In standard ferrofluid models the magnetic moment of a ferrofluid particle is supposed to be fixed with respect to the particle itself, which corresponds to the limit of an infinitely high single-particle magnetic anisotropy. In contrast to this strongly simplifying assumption, we take into account that in real ferrofluids the magnetic moments of ferrofluid particles are allowed to rotate with respect to the particles themselves. Our model results in a system of equations of motion describing both magnetic and mechanical degrees of freedom, where the 'magnetic' equations are coupled with the 'mechanical' equations via (i) the interparticle distances determining the magnetodipolar interaction fields and (ii) orientations of the particle anisotropy axes with respect to their magnetic moments which define the mechanical torque on the particle.

Using our model we have studied the ferrofluid magnetization dynamics for various particle concentrations, i.e., for various magnetodipolar interaction strengths. In particular, we present numerical results (a) the magnetization relaxation of a ferrofluid after the external field is switched off and (b) the frequency dependence of the ferrofluid AC susceptibility. Comparing these results with the corresponding dependences obtained for the rigid dipoles model, we demonstrate that for magnetic anisotropy values typical for commonly used ferrofluid materials (like magnetite) the inclusion of 'magnetic' degrees of freedom is qualitatively essential to obtain a correct description of the ferrofluid dynamics.

Contents

Introduction

In this paper we use a mesoscopic approach for theoretical studies of ferrofluid dynamics. This approach differs from both (i) the microscopic formalism, where a true molecular structure of a ferrofluid (solvent molecules surrounding magnetic particles coated with surfactant molecules) is considered, and (ii) macroscopic phenomenology, where a ferrofluid is considered as a continuum characterized via macroscopic parameters such as average viscosity and magnetic susceptibility, which exhibit a complicated dependence on the applied field and mechanical shear stress. In the mesoscopic treatment a ferrofluid consists of fine magnetic particles immersed into a carrier fluid with a known viscosity. Particles are usually so small that they can be considered as single-domain, i.e., their magnetic moment magnitudes are constant and do not depend on the applied field. The surfactant layer coating each particle is included into the calculation as a non-magnetic particle shell causing a (more or less postulated) repulsive potential. This potential prevents particle aggregation occurring due to the magnetodipolar attraction of magnetic moments by their suitable mutual orientation.

The advantages of this mesoscopic approach are well known: on the one hand, the transition from a microscopic treatment on a molecular level to the formalism where a carrier fluid is considered as a continuous medium and magnetic particles as dipoles with prescribed geometric and magnetic parameters greatly simplifies the problem. From the point of view of numerical simulations presented in this paper this means that the physical volume of the system which can be successfully studied in a reasonable computer time increases by many orders of magnitude. On the other hand, explicitly taking into account the spatial arrangement of particles and directions of their magnetic moments enables the studies of a ferrofluid properties 'nearly from first principles', avoiding hardly controllable *a priori* assumptions concerning the behaviour of the macroscopic ferrofluid characteristics (viscosity and susceptibility) needed to successfully develop a macroscopic theory.

The price to pay for the advantage over a macroscopic approach is a still very high complexity of a system. Several competing short- and long-range interactions make an analytical solution of any realistic problem impossible, so that numerical simulations are required. Among various methods used for simulations of such systems the Langevin dynamics (LD) is a most suitable one, especially by studying *fast* magnetization dynamics, because LD uses the solution of stochastic equations of motion for all relevant ferrofluid degrees of freedom, thus allowing us to include into consideration in a self-consistent way not only all the deterministic interactions between ferrofluid particles, but also the effects of thermal fluctuations.

1. Ferrofluids with internal magnetic degrees of freedom: basic formalism

1.1. Langevin dynamics equations

We begin with the stochastic (Langevin) equations of motion for various degrees of freedom of the ferrofluid particles.

Rotation of the particle magnetic moments. First we point out that, in contrast to virtually all numerical simulations performed on ferrofluids (see, e.g., Davis *et al* 1999, Huang *et al* 2005, Ilg *et al* 2003, Wang *et al* 2002, etc), in our model we explicitly take into account that the magnetic moment of a ferrofluid particle is able to rotate *with respect to the particle itself*, changing its orientation relative to the particle crystallographic axes. We shall see that this additional degree of freedom may qualitatively influence the system behaviour.

The stochastic equation of motion for a magnetic moment $\boldsymbol{\mu}_i$ of the ith particle is (Brown 1963) (below $\gamma > 0$ denotes a gyromagnetic ratio)

$$\frac{\mathrm{d}\boldsymbol{\mu}_i}{\mathrm{d}t} = -\gamma[\boldsymbol{\mu}_i \times (\mathbf{H}_i^{\mathrm{det}} + \mathbf{H}_i^{\mathrm{fl}})] - \gamma\frac{\alpha}{\mu_i}[\boldsymbol{\mu}_i \times [\boldsymbol{\mu}_i \times (\mathbf{H}_i^{\mathrm{det}} + \mathbf{H}_i^{\mathrm{fl}})]]. \tag{1.1}$$

Here the first term describes the moment precession in the total effective field $\mathbf{H}^{\mathrm{tot}} = \mathbf{H}^{\mathrm{det}} + \mathbf{H}^{\mathrm{fl}}$, and the second term accounts for the convergence of this precession trajectory to the direction of $\mathbf{H}^{\mathrm{tot}}$ due to the magnetic energy dissipation. The power of this energy dissipation is controlled by the dimensionless dissipation constant α. The effective field is the sum of the deterministic part $\mathbf{H}^{\mathrm{det}}$ and the thermal field $\mathbf{H}^{\mathrm{fl}}$. The first part includes all magnetic interactions, in case of a ferrofluid represented by an external field $\mathbf{H}^{\mathrm{ext}}$, single-particle anisotropy field $\mathbf{H}^{\mathrm{an}}$ and magnetodipolar interparticle interaction field $\mathbf{H}^{\mathrm{dip}}$. The thermal field $\mathbf{H}^{\mathrm{fl}}$ is constructed to account for thermal fluctuations within a magnetic particle leading to rotational diffusion of its magnetic moment (Brown 1963). The components of $\mathbf{H}^{\mathrm{fl}}$ are time-dependent random variables with correlations defined as for a standard Wiener process:

$$\langle H_{i,\xi}^{\mathrm{fl}}(0) \cdot H_{j,\psi}^{\mathrm{fl}}(t)\rangle = 2D_{\mathrm{mag}} \cdot \delta(t)\delta_{ij}\delta_{\xi\psi}. \tag{1.2}$$

Here i, j denote the particle numbers, $\xi, \psi = x, y, z$ and the noise power depends on the system temperature T and the dissipation constant α: $D_{\mathrm{mag}} = \alpha(1+\alpha^2) \cdot kT/\gamma\mu$.

Translational motion of ferrofluid particles. For particles with sizes ∼10–100 nm and a carrier fluid viscosity ∼0.01–0.1 Ps (both parameters typical for 'standard' ferrofluids) the inertial term for the mechanical motion of particles can safely be neglected. In this approximation the equation describing the translational motion of a ferrofluid particle expresses the balance

between the viscous force $-b \cdot \mathrm{d}\mathbf{r}/\mathrm{d}t$ (b is the viscous friction coefficient) acting on a moving particle and all other forces:

$$b_i \frac{\mathrm{d}\mathbf{r}_i}{\mathrm{d}t} = \mathbf{F}_i^{\mathrm{dip}} + \mathbf{F}_i^{\mathrm{rep}} + \mathbf{F}_i^{\mathrm{hydr}} + \mathbf{F}_i^{\mathrm{fl}} = \nabla(\boldsymbol{\mu}_i \mathbf{H}_i^{\mathrm{dip}}) - \nabla U_i^{\mathrm{rep}} + \mathbf{F}_i^{\mathrm{hydr}} + \mathbf{F}_i^{\mathrm{fl}}. \quad (1.3)$$

These other forces, as was the case for the magnetic moment rotation, can be subdivided into deterministic and the stochastic forces. To the first group belong (i) the magnetodipolar force $\mathbf{F}^{\mathrm{dip}} = -\nabla U^{\mathrm{dip}} = \nabla(\boldsymbol{\mu}\mathbf{H}^{\mathrm{dip}})$, (ii) the steric repulsion force $\mathbf{F}^{\mathrm{rep}} = -\nabla U^{\mathrm{rep}}$ due to the non-magnetic shell surrounding the magnetic particle kernel, and (iii) the hydrodynamic interaction force $\mathbf{F}^{\mathrm{hydr}}$ (see section 4 below). It is important to note that the force due to the *anisotropy* field should *not* appear in the equation describing the translational particle motion, because this force leads to the *rotation* of a magnetic moment, which has no direct influence on the translational particle motion. The stochastic thermal force $\mathbf{F}^{\mathrm{fl}}$ responsible for a translational Brownian motion has *in the absence of the hydrodynamic interactions* conceptually the same simple correlation properties $\langle F_{i,\xi}^{\mathrm{fl}}(0) \cdot F_{j,\psi}^{\mathrm{fl}}(t)\rangle = 2kTb_i \cdot \delta_{ij}\delta_{\xi\psi}\delta(t)$ as the thermal field (1.2). When hydrodynamic interaction is taken into account, the situation changes qualitatively—see the discussion in section 4.

Rotational motion of ferrofluid particles. For the sake of simplicity we assume that a shape of ferrofluid particles is approximately spherical. To describe the rotational motion of such a particle we have to choose some arbitrary axis firmly connected to the particle. For the magnetically simplest situation when every particle possesses a *uniaxial* magnetic anisotropy, we choose this anisotropy axis (whose direction is given by the unit vector $\mathbf{n}_i$) to describe the particle rotation. Without the inertial term the corresponding equation of motion

$$\zeta_i \frac{\mathrm{d}\mathbf{n}_i}{\mathrm{d}t} = [\mathbf{n}_i \times \mathbf{T}_i^{\mathrm{mag}}] - [\mathbf{n}_i \times \mathbf{T}_i^{\mathrm{hydr}}] - [\mathbf{n}_i \times \mathbf{T}_i^{\mathrm{fl}}] \quad (1.4)$$

accounts for the balance between the viscous torque (ζ_i being the rotational viscous friction coefficient) and the other deterministic torques caused by magnetic anisotropy $\mathbf{T}^{\mathrm{mag}} = [\boldsymbol{\mu} \times \mathbf{H}^{\mathrm{an}}]$, hydrodynamical interaction $\mathbf{T}^{\mathrm{hydr}}$ and the random torque $\mathbf{T}^{\mathrm{fl}}$ due to the thermal bath fluctuations. Again, if hydrodynamical interactions can be neglected, the components of $\mathbf{T}^{\mathrm{fl}}$ have the same simple correlation properties $\langle T_{i,\xi}^{\mathrm{fl}}(t) \cdot T_{j,\psi}^{\mathrm{fl}}(t')\rangle = 2kT\zeta_i \cdot \delta_{ij}\delta_{\xi\psi}\delta(t-t')$.

We point out that the *magnetodipolar* interaction does not explicitly lead to a torque acting on the *particle*: the corresponding field is applied to the *magnetic moment* of the particle. The influence of this field on the rotational particle motion thus manifests itself in the change of the magnetic moment orientation which leads to the change of the *anisotropy* torque. The latter influence is already taken into account by the first term on the right-hand side of (1.4).

1.2. Relation between 'magnetic' and 'mechanical' times

Straightforward numerical integration of the system of Langevin equations (1.1), (1.3) and (1.4) is extremely inefficient, which can be seen already after rewriting these equations in suitable reduced units.

Convenient 'magnetic' units are the reduced particle moment $\mathbf{m}_i = \boldsymbol{\mu}_i/\mu_i = \boldsymbol{\mu}_i/M_{\mathrm{S}}V_i$ (here M_{S} is the particle saturation magnetization and V_i its volume, so $|\mathbf{m}_i| = 1$), reduced field $\mathbf{h} = \mathbf{H}/M_{\mathrm{S}}$ and reduced anisotropy constant $\beta = 2K/M_{\mathrm{S}}^2$. In the last definition K is the 'normal' anisotropy constant from the anisotropy energy expressions like $E^{\mathrm{an}} = KV_i \sin^2(\mathbf{m}_i\mathbf{n}_i)$ for the uniaxial anisotropy case, so that the value of this reduced anisotropy β gives the relation of the anisotropy field to the maximal dipolar interaction field (from the

Table 1. Dynamic processes and corresponding typical times for *magnetic* degrees of freedom in a ferrofluid.

Process kind	General formula for its characteristic time $t_{\rm char}$	Expression for $t_{\rm char}$ via 'magnetic' time, material and external parameters	$t_{\rm char}$ for typical parameter values
Precession in an effective field $\mathbf{H}_{\rm eff}$	$t_{\rm prec} \sim \frac{1}{\omega_0} = \frac{1}{\gamma H_{\rm eff}}$	$t_{\rm prec} \sim \frac{1}{\gamma M_{\rm S}} \frac{M_{\rm S}}{H_{\rm eff}} = t_{\rm mag} \frac{M_{\rm S}}{H_{\rm eff}}$	$t_{\rm prec} \sim 10^{-10}$ s
Relaxation towards $\mathbf{H}_{\rm eff}$	$t_{\rm rel}^{\rm mag} \sim \frac{1}{\lambda} \cdot \frac{1}{\gamma H_{\rm eff}}$	$t_{\rm rel}^{\rm mag} \sim \frac{1}{\lambda} \cdot t_{\rm mag} \cdot \frac{M_{\rm S}}{H_{\rm eff}}$	$t_{\rm rel}^{\rm mag} \sim 10^{-9}$ s
Rotational diffusion of a magnetic moment	$t_{\rm diff}^{\rm mag} \sim \frac{1}{\lambda} \cdot \frac{1}{\gamma M_{\rm S}} \cdot \frac{M_{\rm S}^2 V_{\rm p}}{kT}$	$t_{\rm diff}^{\rm mag} \sim \frac{1}{\lambda} \cdot \frac{t_{\rm mag}}{\Theta}$	$t_{\rm diff}^{\rm mag} \sim 3 \times 10^{-9}$ s
Jump over the energy barrier (Néel relaxation)	$t_{\rm Neel} \sim t_{\rm diff}^{\rm mag} \cdot \exp\left\{\frac{\Delta E}{kT}\right\}$	$t_{\rm Neel} \sim t_{\rm diff}^{\rm mag} \cdot \exp\left\{\frac{\beta}{2\Theta}\right\}$	**Arbitrary**

nearest possible neighbour). In these units the Langevin equation for the magnetic moment motion is

$$t_{\rm mag} \cdot \frac{{\rm d}\mathbf{m}_i}{{\rm d}t} = -[\mathbf{m}_i \times (\mathbf{h}_i^{\rm det} + \mathbf{h}_i^{\rm fl})] - \alpha[\mathbf{m}_i \times [\mathbf{m}_i \times (\mathbf{h}_i^{\rm det} + \mathbf{h}_i^{\rm fl})]] \qquad (1.1b)$$

where the 'magnetic time' is defined as $t_{\rm mag} = 1/\gamma M_{\rm S}$ ($\gamma \approx 1.76 \times 10^7$ G s^{-1} is the gyromagnetic ratio). For a typical ferrofluid made from magnetite ($M_{\rm S} \approx 400$ G) particles, $t_{\rm mag} \approx 1.4 \times 10^{-10}$ s.

To construct convenient mechanical reduced units, we use as a natural length the *average* radius of the magnetic particle kernel $R_{\rm av}$, so that the reduced full particle radius (kernel radius $R_{\rm mag}$ plus shell thickness $h_{\rm sh}$) is $\mathbf{r}_i^{\rm tot} = (R_{{\rm mag},i} + h_{\rm sh})/R_{\rm av}$, the reduced radius-vector of a particle position is $\mathbf{s}_i = \mathbf{r}_i/R_{\rm av}$ and the reduced volume $v_i = V_i/R_{\rm av}^3$. A convenient energy unit is the demagnetizing self-energy $E^{\rm dem} = V_{\rm av} M_{\rm S}^2$ of the particle with the average radius $R_{\rm av}$, which gives the reduced force defined as $\mathbf{f} = \mathbf{F} \cdot R_{\rm av}/E^{\rm dem} = \mathbf{F} \cdot R_{\rm av}/V_{\rm av} M_{\rm S}^2$ and reduced temperature $\Theta = kT/V_{\rm av} M_{\rm S}^2$. Stochastic equations for translational and rotational particle motions can be written in these reduced units as

$$\frac{9}{2} t_{\rm visc} \cdot \rho_i^{\rm tot} \frac{{\rm d}\mathbf{s}_i}{{\rm d}t} = v_i \cdot \nabla_{\mathbf{s}}(\mathbf{m}_i \mathbf{h}_i^{\rm dip}) - \nabla u_i^{\rm rep} + \mathbf{f}_i^{\rm hydr} + \mathbf{f}_i^{\rm fl} \qquad (1.3b)$$

$$6 t_{\rm visc} \cdot (\rho_i^{\rm tot})^3 \cdot \frac{{\rm d}\mathbf{n}_i}{{\rm d}t} = v_i \cdot [\mathbf{n}_i \times [\mathbf{m}_i \times \mathbf{h}_i^{\rm an}]] - [\mathbf{n}_i \times {\rm T}_i^{\rm hydr}] - [\mathbf{n}_i \times {\rm T}_i^{\rm fl}] \qquad (1.4b)$$

where the 'viscous' time $t_{\rm visc} = \eta/M_{\rm S}^2$ (η denotes the viscosity of the carrier fluid). Equations (1.3*b*) and (1.4*b*) use explicitly the above-mentioned assumption that the particle is a sphere with the hydrodynamic radius $R_{\rm hyd} = R_{\rm p} + h_{\rm sh}$, so that the translational b and rotational ζ viscous friction coefficients are $b = 6\pi\eta R_{\rm hyd}$ and $\zeta = 8\pi\eta R_{\rm hyd}^3$. For a typical water-based magnetite ferrofluid ($\eta \approx 10^{-2}$ P, $M_{\rm S} \approx 400$ G) we obtain $t_{\rm visc} \approx 0.6 \times 10^{-7}$ s.

A quick inspection of the equations of motion ((1.1*b*), (1.3*b*), (1.4*b*)) written in reduced units suggests that 'magnetic' and 'viscous' times $t_{\rm mag}$ and $t_{\rm visc}$ represent typical timescales characterizing the motion associated with the corresponding degrees of freedom. This would mean that in a ferrofluid the magnetic subsystem relaxes much faster than the mechanical one, simply because $t_{\rm mag}$ ($\sim 10^{-10}$ s) $\ll$ $t_{\rm visc}$ (10^{-7} s). The situation is, however, much more complicated due to many different kinds of dynamic processes involved. Typical timescales characterizing all these processes should be analysed before one can proceed with the elaboration of numerical algorithms suitable for the simulations using the basic Langevin equations (1.1), (1.3), (1.4).

Although the expressions for these characteristic times given in tables 1 and 2 are mostly self-explanatory, we shall briefly comment on each time listed there.

Table 2. Dynamic processes and corresponding timescales for the *mechanical* motion of ferrofluid particles.

Process kind	General formula for its characteristic time t_{char}	Expression for t_{char} via 'viscous' time, material and external parameters	t_{char} for typical parameter values
Deterministic translational motion	$t^{\text{det}}_{\text{trans}} \sim \frac{R_{\text{mag}}}{v_{\text{trans}}} \sim R_{\text{mag}} \frac{b_{\text{trans}}}{F_{\text{det}}}$	$t^{\text{det}}_{\text{trans}} \sim t_{\text{visc}} \cdot (1+\tilde{h})^5$	$t^{\text{det}}_{\text{trans}} \sim 2 \times 10^{-6}$ s
Translational diffusion	$t^{\text{diff}}_{\text{trans}} \sim \frac{\langle \Delta r_{\text{diff}} \rangle^2}{D_{\text{trans}}} \sim \frac{R^2_{\text{mag}}}{kT/b_{\text{trans}}}$	$t^{\text{diff}}_{\text{trans}} \sim \frac{9}{2} \cdot \frac{t_{\text{visc}}}{\Theta} \cdot (1+\tilde{h})$	$t^{\text{diff}}_{\text{trans}} \sim 10^{-6}$ s
Deterministic particle rotation	$t^{\text{det}}_{\text{rot}} \sim \frac{1}{\omega_{\text{rot}}} \sim \frac{\zeta_{\text{rot}}}{T_{\text{det}}}$	$t^{\text{det}}_{\text{rot}} \sim \frac{t_{\text{visc}}}{\beta} \cdot (1+\tilde{h})^3$	$t^{\text{det}}_{\text{rot}} \sim 10^{-6}$ s
Rotational diffusion	$t^{\text{diff}}_{\text{rot}} \sim \frac{1}{D_{\text{rot}}} \sim \frac{\zeta_{\text{rot}}}{kT}$	$t^{\text{diff}}_{\text{rot}} \sim 6 \cdot \frac{t_{\text{visc}}}{\Theta} \cdot (1+\tilde{h})^3$	$t^{\text{diff}}_{\text{rot}} \sim 5 \times 10^{-6}$ s

Dynamic processes where magnetic moments are involved and their characteristic times (i.e., relaxation times of 'magnetic' degrees of freedom) are collected in table 1. The timescale for the moment *precession* (first row) is simply deduced from the textbook result for the precession frequency of a magnetic moment in an given effective field ($\omega = \gamma H$) and then rewritten to make explicit use of the magnetic time $t_{\text{mag}} = 1/\gamma M_{\text{S}}$ defined above, because the latter time is a *material* parameter. The expression in the second row for the *relaxation time of a magnetic moment towards the effective field direction* (due to the energy dissipation whose rate is given by the dissipation constant λ) is valid for the most common case $\lambda \ll 1$; the corresponding derivation can be found in Coffey *et al* (1996). The *rotational diffusion time* of a magnetic moment (third row) characterizes its chaotic motion due to thermal fluctuations in the absence of any external field and anisotropy (Coffey *et al* 1996) and hence depends only on the dissipation λ, particle saturation magnetization M_{S} and system temperature T.

The most complicated process is a thermally activated *transition of a magnetic moment over an energy barrier* in a system with more than one local energy minimum. If the two minima are separated by the energy barrier ΔE then for $\Delta E \gg kT$ the average transition time depends in a very good approximation exponentially from the relation $\Delta E/kT$ (Arrhenius law, see Hoenggi *et al* (1990) for details) as indicated in the second column of the last row in table 1. The origin of the energy barrier determines its dependence on the system parameters. In particular, for a single magnetic particle with the uniaxial anisotropy energy $E^{\text{an}} = K V_{\text{mag}} \sin^2\theta$ (where V_{mag} is the volume of a magnetic particle kernel, K the anisotropy constant and θ the angle between the particle moment $\mathbf{m}$ and the anisotropy axis direction $\mathbf{n}$) the two equivalent energy minima (achieved for $\mathbf{m} \uparrow\uparrow \mathbf{n}$ or $\mathbf{m} \uparrow\downarrow \mathbf{n}$) are separated by the energy barrier $\Delta E = KV$. In this case the relation $\Delta E/kT$ can be conveniently expressed in terms of the reduced anisotropy β and temperature Θ as shown in the third column of the last row.

Values of the corresponding characteristic times given in the last table column are computed for the typical parameters of a water-based magnetite ferrofluid (diameter of a particle magnetic kernel $D_{\text{mag}} = 10$ nm, particle saturation magnetization $M_{\text{S}} = 400$ G, reduced anisotropy $\beta = 0.5$, dissipation constant $\lambda = 0.1$) and external conditions (magnetic field $H \sim M_{\text{S}}$ and temperature $T = 300$ K). It can be seen that for the first three kinds of dynamic process these times are in the range $\sim 10^{-9}$–10^{-10} s, which is mainly due to a very high moment precession frequency ($\sim$10 GHz) for typical magnetic materials. Additional factors coming from the dissipation constant λ and reduced temperature Θ ($\sim$1 for the parameter values listed above) have a minor influence on these time values.

However, there exists an important exception—the characteristic time for the Néel relaxation represented in table 1 with a bold question mark. This question mark means that the exponential dependence of this time on the energy barrier (and the system temperature)

does not allow us to give even a rough estimate of this time for a realistic system. In particular, if the energy barrier arises, as in the example above, from the single-particle anisotropy, then a very moderate distribution of particle sizes present in every real ferrofluid (even neglecting the distribution of anisotropy constants and the interparticle interaction) leads to a huge dispersion of the corresponding transition times: due to the cubic dependence of the particle volume (and hence the energy barrier height) on the particle size, doubling the particle diameter from 10 to 20 nm (for other parameter values as given above) increases t_{Neel} by nearly two orders of magnitude—from 3×10^{-9} up to 10^{-7} s. This circumstance turns out to be very important by the development of an efficient algorithm for the handling of the ferrofluid Langevin dynamics, as will be discussed below. But before this discussion we briefly turn our attention to the estimation of the 'mechanical' relaxation times.

Corresponding dynamic processes involving deterministic translational and rotational motions as well as translational and rotational diffusion are collected in table 2. Characteristic times for the deterministic translational particle motion (translational diffusion) are defined as times during which a particle passes a characteristic distance within a system in process of its deterministic motion (diffusion). As a natural characteristic distance we choose the radius of a magnetic particle kernel R_{mag}, thus obtaining the simple estimates given in the second column of table 2 (v_{trans} is the velocity of a particle with the friction coefficient b_{trans} under the influence of a deterministic force F_{det} and D_{trans} is the translational diffusion coefficient). As a deterministic force acting on the particle we consider the magnetodipolar force which depends on the particle moment and interparticle distance as $F_{\mathrm{det}} = F_{\mathrm{dip}} \sim \mu^2/r_{ij}^4$. We have chosen this interaction because, in contrast to the steric repulsion, it is a long-range one, and thus influences the particle motion not only during the particle collisions. Resulting expressions for the characteristic 'translational' times are given in the third column. The factors $(1 + \tilde{h})$ containing the ratio $\tilde{h} = h/R_{\mathrm{mag}}$ of the particle shell thickness to its magnetic kernel radius appear naturally because the magnetic moment value μ and the reduced temperature Θ are defined via the particle *magnetic* volume $V_{\mathrm{mag}} \sim R_{\mathrm{mag}}^3$, whereas the friction coefficient b_{trans} and the minimal interparticle distance r_{ij} contain the total particle radius $R_{\mathrm{mag}}+h$. The presence of this factor may be important for ferrofluids composed of very small particles where the shell thickness is comparable to the particle size.

Estimation for typical times of the deterministic particle rotation and rotational diffusion (the two last rows in the table 2) are obtained in a similar fashion assuming a characteristic rotation angle $\sim$1 rad for a particle with the rotational friction and diffusion coefficients ζ_{rot} and D_{rot}. As a deterministic torque we have chosen the magnetic anisotropy torque $\mathbf{T}_{\mathrm{mag}}$, which explains the appearance of the reduced anisotropy constant β in the expression for $t_{\mathrm{rot}}^{\mathrm{det}}$.

Numerical values of all 'mechanical' times given in the last table column are calculated using the same parameters as 'magnetic' times. In addition, we have assumed a relatively thick shell $h \approx R_{\mathrm{mag}}$ to demonstrate the effect of this parameter (note that $t_{\mathrm{trans}}^{\mathrm{det}}$ is much larger than $t_{\mathrm{trans}}^{\mathrm{diff}}$ despite $\Theta \sim 1$) and the carrier fluid viscosity $\eta = 10^{-2}$ P (water).

1.3. Optimal simulation algorithms for various physical situations

The first conclusion which can be immediately drawn from the comparison of magnetic and mechanical characteristic times presented in the tables above is that, except for the Néel relaxation, all magnetic degrees of freedom relax much faster than the mechanical ones. For this reason direct integration of the basic equations (1.1)–(1.4) is very inefficient in any case, because the overwhelming majority of the computer time would be spent following the rapid magnetic relaxation (mainly precession) according to equation (1.1), whereby the particles would remain nearly immobile, as was already pointed out in Berkov *et al* (2003). On the

other hand, we cannot simply treat magnetic relaxation as being always much faster than the mechanical motion, because the Néel relaxation time could be arbitrary large, as discussed above.

For this reason we have to analyse the relation between various energy scales relevant for magnetic fluids and between corresponding relaxation times in order to construct an optimal algorithm for every specific case.

Leaving aside the energy due to the steric repulsion potential (this short-range interaction is assumed to act only during the direction particle collisions), we can distinguish between the following characteristic energies for our system:

- Demagnetizing energy $E_{\rm dem} \sim M_{\rm S}^2 V_{\rm mag}$ of a single particle, which was used above to construct the reduced temperature Θ. This is the self-interaction energy of the particle magnetization with the magnetic field created by the same particle. For a spherical particle this interaction does not depend on the moment orientation and hence is not important for a real dynamic process, but the parameter combination by itself gives a good basis for the analysis of other energy kinds (see below).
- Single-particle anisotropy energy $E_{\rm an} \sim KV_{\rm mag} = \frac{\beta}{2} M_{\rm S}^2 V_{\rm mag} = \frac{\beta}{2} E_{\rm dem}$. This value gives the energy barrier height between the two local minima of the anisotropy energy of a magnetic moment for a particle with uniaxial anisotropy.
- Maximal dipolar interaction energy $E_{\rm dip}^{\rm max} \sim \mu H_{\rm dip}^{\rm max} \simeq \frac{\mu^2}{r_{\rm min}^3} = \frac{(M_{\rm S} V_{\rm mag})^2}{(2R_{\rm part})^3} \sim E_{\rm dem}$. This is the energy of the magnetodipolar interaction for two particles at the minimum possible distance and it has the same order of magnitude as the self-energy $E_{\rm dem}$ simply because the minimal distance between two coated ferrofluid particles is approximately the same as the diameter of their magnetic kernels.
- Thermal fluctuation energy $E_{\rm T} = kT$.

The relation between the anisotropy energy $E_{\rm an}$ and the magnetodipolar interaction energy $E_{\rm dip}$ determines the importance of the interaction effects: for $E_{\rm an} \gg E_{\rm dem}$, i.e., for large reduced anisotropy $\beta \gg 1$, the dipolar interaction is weak and may be taken into account in the random field approximation or even neglected.

The relation between the energy barrier height for magnetic relaxation $DE_{\rm mag}$ and the thermal energy kT determines the Néel relaxation time $t_{\rm Neel} = t_{\rm diff}^{\rm mag} \cdot \exp(\Delta E/kT)$ and thus controls the relation between this time and 'mechanical' times given by $t_{\rm visc}$. In the simplest case when the magnetic relaxation barrier is determined by the single particle anisotropy, the Néel time is determined by the relation between the reduced anisotropy β and reduced temperature Θ: $\Delta E_{\rm an}/kT = KV/kT = (\beta/2) \cdot (M_{\rm S}^2 V_{\rm mag}/kT) = \beta/2\Theta$. We can neglect the Néel relaxation, if the corresponding relaxation time is larger (strictly speaking, much larger) than the characteristic mechanical motion times, i.e., if $t_{\rm Neel} = t_{\rm diff}^{\rm mag} \cdot \exp(\Delta E/kT) \gg t_{\rm visc}$. For the single-particle anisotropy barrier this condition means that the inequality

$$\frac{\beta}{\Theta} \gg 2 \ln \left(\frac{t_{\rm visc}}{t_{\rm diff}^{\rm mag}} \right) \tag{1.5}$$

should be fulfilled.

Based on the energy considerations presented above, we can draw a convenient phase diagram for the visualization of ferrofluid parameter areas where certain processes may or may not be neglected. Suitable variables for this diagram are (i) the reduced anisotropy constant $\beta = 2K/M_{\rm S}^2$, which controls both the importance of magnetodipolar interaction effects and the height of the energy barriers, and (ii) the ratio of the demagnetizing and thermal energy $\tilde{E}_{\rm dem} = E_{\rm dem}/kT = M_{\rm S}^2 V_{\rm mag}/kT = 1/\Theta$. Taking into account that the saturation magnetization $M_{\rm S}$ for different magnetic materials varies mostly in a quite narrow region from

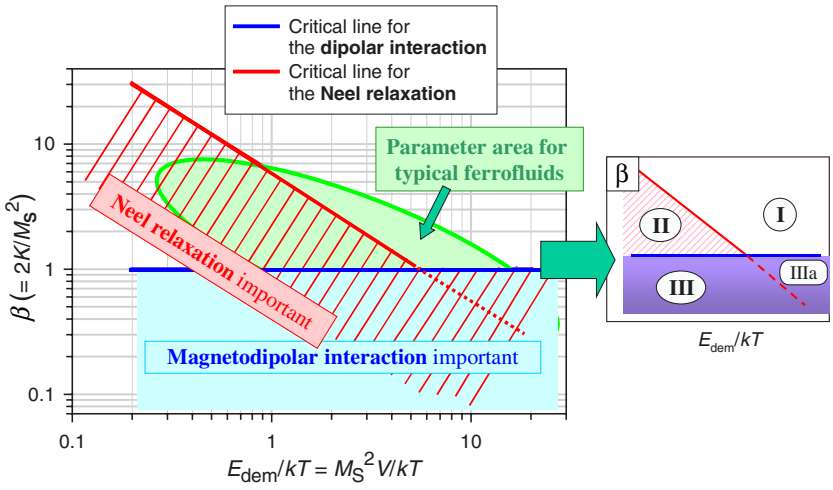

Figure 1. Phase diagram showing where the magnetodipolar interaction effect (below the blue line) and Néel relaxation (below the red line) are important together with the region of particle parameters for typical ferrofluids (green elliptical area). The picture on the right shows the parameter areas where different numerical algorithms should be applied—see text for details.

300 to 1000 G and the temperature entering into the second variable is nearly always equal to the room temperature $T = 300$ K, this diagram can be also viewed as a diagram in anisotropy–particle volume coordinates.

The resulting diagram is presented in figure 1 (note the logarithmic scales of both axes!). The horizontal blue line $\beta = 1$ separates the region where magnetodipolar interaction effects are important (below this line) from the parameter area where single-particle anisotropy dominates. Correspondingly the hyperbola (1.5) $\beta E_{\rm dem} = 2\ln(t_{\rm visc}/t_{\rm diff}^{\rm mag}) \equiv C_N \approx 6$ (the value of C_N is computed for system parameters used for the tables 1 and 2) confines the region where the Néel relaxation should be taken into account[3] (in the single-particle approximation).

The particle parameter region for typical ferrofluids (e.g., magnetite, maghemite and Co) is roughly shown in the same picture as a green ellipse. Drawing this area we (a) have taken into account that the ferrofluid particle diameters mostly lie in the range 5 nm $\leqslant D_{\rm mag} \leqslant$ 20 nm and (b) have analysed many experimental studies showing that the range of reduced particle anisotropy is normally $0.5 \leqslant \beta \leqslant 5$. The slope of the ellipse indicates the well known fact that the total anisotropy usually increases with decreasing the particle size, because the contribution of the strong surface anisotropy becomes more important.

The division of the particle parameter plane $(\beta, \tilde{E}_{\rm dem})$ into the four regions as shown in figure 1 provides a convenient basis for developing reliable simulation algorithms. We consider all these regions marked in figure 1 as I, II, IIIa and IIIb in the order of appearance.

- *In region I* the Néel relaxation is negligible and magnetodipolar interaction is much smaller than the anisotropy field. This means that the rotation of the magnetic moment with respect to the particle itself can be neglected, or, in other words, *the model of rigid dipoles* (dipoles 'firmly attached' to particles) is applicable. In this case the first Langevin equation (1.1) can be omitted; the anisotropy field in the magnetic torque $\mathbf{T}^{\rm mag}$ in equation (1.4) should be replaced by the dipolar field $\mathbf{H}^{\rm dip}$, because the moment is assumed to be 'attached'

[3] We note in passing that although the concrete value of the ratio $t_{\rm visc}/t_{\rm diff}^{\rm mag}$ depends, of course, on the particle magnetization and some other parameters, the logarithmic dependence of the constant $C_{\rm N}$ (which determines the exact position of the hyperbola) on this ratio makes its dependence on these parameters negligible.

to the anisotropy axis, so that the torque on the particle comes now from the dipolar field acting on this moment. After this omission and replacement one is left with a technically demanding, but conceptually simple task of solving the system of Langevin equations (1.3), (1.4), as was done in nearly all papers devoted to numerical simulations of ferrofluids including thermal fluctuation effects.

- *In region II* the situation is slightly more complicated. The dipolar interaction is still much weaker than the anisotropy field, so that the particle moment is oriented almost along its anisotropy axis. However, due to the small particle volume the anisotropy energy barrier is comparable with the thermal energy and hence moment jumps between the two equivalent directions of the anisotropy axis (Néel relaxation) are possible (*model of rigid dipoles with random flips*). There is still no need to solve explicitly equation (1.1) to include these jumps: they can be taken into account during the solution of the mechanical Langevin equations as discrete events which happen with the probability p evaluated from the Arrhenius law ($p \sim \exp(-KV/kT)$). This situation is expected for ferrofluids consisting of very small particles ($D_{\mathrm{mag}} \leqslant 5$ nm) with high single-particle anisotropy ($\beta \geqslant 2$).
- *The region of the phase diagram below the line* $\beta = 1$ (where the dipolar field is comparable with or larger than the anisotropy field is apparently divided further into two regions—IIIa, where the Néel relaxation is important, and IIIb, where this relaxation seems to be negligible because $\Delta E \gg kT$. However, we point out that the energy barrier in the region IIIb was estimated as a *single-particle anisotropy barrier* without taking into account magnetodipolar interaction. We have shown in Berkov (2002) that for $\beta \leqslant 2$ this interaction significantly changes the energy barrier heights, and already for very moderate particle volume concentration ($c \geqslant 0.05$) ΔE significantly decreases for a large fraction of particles. For this reason the Néel relaxation in this parameter region cannot really be neglected, which is indicated by the red hatching of this area in figure 1.

For this reason for the whole parameter region which is below either the red hyperbola or the blue straight line in figure 1 the rigorous solution of the complete system (1.1)–(1.4) is necessary. However, the separation of timescales into fast magnetic precession and relatively slow mechanical motion can be used for the important optimization of the solution method. Namely, the time step by the integration of the 'magnetic' equation (1.1) is necessarily much smaller than the time step required to follow the mechanical motion described by (1.3), (1.4). Hence the displacement of particles during a 'magnetic' step is going to be negligibly small, which allows us to adopt the following strategy: using some kind of an algorithm with an adaptive step-size control for the solution for mechanical equation, we first predict the time interval Δt_{mech} for the next 'mechanical' step. Afterwards we integrate the 'magnetic' Langevin equation during this time Δt_{mech} (using, as explained above, much smaller 'magnetic' steps) neglecting the mechanical motion of particles. During this integration we evaluate *the time-averaged values* of magnetic moments and torques which are then substituted into the 'mechanical' equations to evaluate the forces and torques required to make a 'mechanical' step.

This method allows us to accelerate the calculations by several times even when the hydrodynamic interaction is neglected, so that the major part of the computer time is spent for the evaluation of the magnetodipolar interaction. The reason is that when we neglect the mechanical motion during the integration of the magnetic moment trajectories, we can evaluate and store at the end of each previous mechanical step all the position-dependent dipolar interaction coefficients in the expression for the magnetodipolar interaction, so that only the moment orientations must be updated. And for the hydrodynamic interaction included the most time-consuming step is the evaluation of mechanical thermal fluctuation forces and torques, which are correlated due to the hydrodynamic interaction (see the corresponding

section below). Such an evaluation requires $\sim N^3$ iterations due to the matrix decomposition involved in the generation of arbitrary correlated random numbers. For this reason the re-evaluation of the particle positions/orientations and corresponding fluctuation forces/torques for each 'magnetic' step would make the whole method absolutely impractical.

2. Overview of the interparticle interactions in a ferrofluid

Ferrofluids belong to the most complicated systems among the colloids, because there exist several entirely different interaction types between the ferrofluid particles: (i) short-range repulsive interaction due to the presence of the coating layer on (ideally) each ferrofluid particle; (ii) long-range anisotropic magnetodipolar interaction between magnetic moments of ferrofluid particles; and (iii) long-range anisotropic hydrodynamic interaction arising because each moving particle induces a stream in the surrounding fluid and this stream acts on all other particles. In this section we briefly review all these interactions, leaving the detailed analysis of the long-range ones to sections 3 and 4.

The short-range steric particle repulsion is the simplest interaction from the simulation point of view, because the calculation of any short-range force for the whole system requires only $\sim N$ operations (N is the particle number) due to the possibility to introduce a final (and in most cases even small) cut-off radius R_{cut} for such an interaction. Unfortunately, the form of the corresponding repulsion potential U^{rep} is still a subject of a controversial debate (see, e.g., Jund *et al* (1995) and reference therein). The two most commonly used forms are the Lennard-Jones potential $U(r) = a/r^{12} - b/r^6$ (where the first term provides the required repulsion) and the Yukawa exponential form $U(r) = A \cdot \exp(-r/r_c)$. The Lennard-Jones expression was suggested a long time ago simply to accelerate the computation of the short-range potential: when the attraction term $-1/r^6$ (which can be shown to result from the self-consistent fluctuations of the electrical dipolar moments for neutral molecules) is already calculated, the repulsion term can be computed very quickly as its square: $1/r^{12} = (1/r^6)^2$. The Yukawa potential can in principle be derived as the potential of an electrical double layer of from the Debye–Hückel theory of strong electrolytes, but neither of these justifications if valid at least for an organic-solvent-based ferrofluid with magnetic particles coated by a neutral polymer shell (the situation for water-based ferrofluids with particles coated by hydrophile surfactants requires a special analysis).

Because the actual form of U^{rep} is unknown, we can choose an arbitrary analytical expression based on several physically plausible requirements: (i) isotropy, (ii) short-range character, and (iii) strong dependence on the interparticle distance (stronger than for magnetodipolar attraction). We have chosen the following exponential form which satisfies all these assumptions:

$$U^{\mathrm{rep}}(r_{ij}) = A \cdot \exp\left(-\frac{r_{ij} - (R_i^{\mathrm{mag}} + R_j^{\mathrm{mag}})}{\delta_c}\right) + C. \tag{2.1}$$

The potential decay radius δ_c should have the same order of magnitude as the particle shell thickness. The prefactor A should ensure that $U^{\mathrm{rep}}(R_i^{\mathrm{mag}} + R_j^{\mathrm{mag}}) \gg E_{\max}^{\mathrm{dip}}(R_i^{\mathrm{mag}} + R_j^{\mathrm{mag}})$ (the maximal dipolar interaction energy for two identical particles is $E_{\max}^{\mathrm{dip}} = (\pi/3)M_{\mathrm{S}}^2 V_{\mathrm{p}}$). The cut-off radius for this potential $R_{\mathrm{cut}}^{\mathrm{rep}}$ should satisfy the condition $R_{\mathrm{cut}}^{\mathrm{rep}} - 2\max_{i=1\ldots N}\{R_i\} \gg \delta_{\mathrm{c}}$. The constant C in (2.1) should in principle be present to avoid a potential jump at $r = R_{\mathrm{cut}}^{\mathrm{rep}}$; its value, however, has no influence on the system dynamics, because the repulsion force in equation (1.2) is evaluated as $\mathbf{F}^{\mathrm{rep}} = -\nabla U^{\mathrm{rep}}$.

Magnetodipolar interaction, in contrast to the steric repulsion, is a long-range interaction. This means that the cut-off of this interaction is, strictly speaking, not allowed. However, as

we shall explain in section 3.1, in many cases the Lorentz cavity (reaction field) method, which uses such a cut-off procedure with some modifications, provides adequate results. In a general case one has to resort to more advanced methods which fully take into account the long-range character of the magnetodipolar field, i.e., to the Ewald or Fast Multipole methods. These methods are discussed in detail in sections 3.2 and 3.3 correspondingly.

Hydrodynamic interaction (HD-interaction), resulting, as explained above, from the particle-induced motion of the carrier fluid, is very different from all other interactions in the system from two points of view. First, it is a so-called purely dissipative interaction, i.e., the hydrodynamic interaction force appears for *moving* particles only and is proportional to the particle velocities. For this reason HD-interaction does not enter into the potential energy of a system (which by its definition may not depend on the particle *velocities*). Thus the *equilibrium* thermodynamical properties of a ferrofluid (like its magnetization in the constant external field as a function of temperature $M(H, T)$) do not depend on whether the HD-interaction is taken into account or not. The second peculiarity of this interaction is a direct consequence of its dissipative character: as will be shown in section 3.3, the very presence of a hydrodynamic interaction leads to long-range correlations between thermal bath fluctuations on various ferrofluid particles, which appear in the 'mechanic' Langevin equations (1.3) and (1.4) as thermal fluctuation forces (torques). The generation of correspondingly correlated random numbers, which is necessary to produce physically correct thermal fluctuations of the particle motion, is very time consuming, because it amounts to the decomposition of a correlation matrix ($\sim Z^3$ operation for an $Z \times Z$ matrix). We shall return to this question in more detail in section 3.3.

3. Methods for calculating the magnetodipolar interaction

The problem of the evaluation of the long-range dipolar field is especially difficult for a ferrofluid, because it represents a disordered particle system, where this spatial disorder prevents a direct application of the lattice-based fast Fourier transformation (FFT). FFT-based algorithms provide the fastest possibility to handle the dipolar interaction both in systems with open boundary conditions (BCs), where they are used for a direct summation and periodic BCs, where they are employed as a part of the lattice Ewald methods. In disordered systems where the translational symmetry of particle positions is absent, one can either apply the fast multipole method (FMM) (Greengard 1988) or map the initial system onto a regular lattice, where the interaction field can be computed using the lattice Ewald procedure and then mapped back to initial particle positions (particle-mesh Ewald methods). For systems with $1/r$-interaction (gravitational and Coulomb forces) corresponding FMM and particle-mesh Ewald methods are well known (Greengard 1988, Hockney and Eastwood 1981). In this section we will present these methods for *dipolar* systems, but first we briefly discuss a much simpler Lorentz cavity method which may be applied in many physically meaningful cases.

3.1. Lorentz cavity (reaction field) method

The idea of this method, which actually uses the modified cut-off procedure, is based on the textbook result that the stray field of a *homogeneously* magnetized media within a spherical *cavity* (Lorentz cavity) cut out inside this media is also homogeneous: $\mathbf{H}_{\rm dip} = 4\pi\mathbf{M}/3$ (note the plus sign of this expression in contrast to the stray field *inside* a homogeneously magnetized sphere in vacuum!). If on some typical length scale $l_{\rm char}$ the magnetization of our magnetic system can be considered as homogeneous, than one can calculate the dipolar field on the given particle taking an *explicit* sum over all other particles inside the sphere with the radius

$R_{\rm cut}^{\rm dip} \geqslant l_{\rm char}$ around this given particle and adding afterwards the contribution of particles outside the sphere as the Lorentz term:

$$\mathbf{H}_i^{\rm dip} = \sum_{j\neq i}^{r_{ij}\leqslant R_{\rm cut}^{\rm dip}} \frac{3\mathbf{e}_{ij}\cdot(\mathbf{e}_{ij}\mathbf{m}_{ij}) - \mathbf{m}_{ij}}{r_{ij}^3} + \frac{4\pi}{3}\langle\mathbf{M}\rangle\,. \tag{3.1}$$

The advantages of the method are obvious. First, it is conceptually very simple. Second, its operation count is linear in the particle number N, because the properly chosen cut-off radius does not depend on the system size and hence the average number of particles $L_{\rm nb}$ within the cut-off sphere (which are called neighbours in this formalism) is constant, so that the number of operations needed to calculate the dipolar field on all particles is $\sim L_{\rm nb}\cdot N$. Third, there exists a standard recipe for choosing $R_{\rm cut}^{\rm dip}$: one should start with $l_{\rm char}$ and increase the cut-off radius until the result does not change any more (within statistical errors, of course). For our specific case-disordered system of fine magnetic particles the obvious characteristic length is the average interparticle distance $\langle\Delta r\rangle$. For system of randomly placed particles we have shown (Berkov and Gorn 2001) that already $R_{\rm cut}^{\rm dip} = 2\langle\Delta r\rangle$ is large enough to provide cut-off-independent results even for such a subtle quantity as AC susceptibility.

However, one should be aware of the obvious limitation of the method, which is the direct consequence of the assumption that the medium is homogeneously magnetized on a corresponding length scale. If particles form *spatial structures whose characteristic size is comparable with the side of the simulation box*, then the Lorentz method badly fails and one should use other algorithms which explicitly take into account the positions of all particles in the system to compute $\mathbf{H}^{\rm dip}$ on the given particle (see sections 3.2 and 3.3 below). Obvious examples of such situations are the formation of (i) long magnetic particle chains in an external field or (ii) aggregates of various shapes in the absence of external field when the particles are so large that thermal fluctuations and coating cannot prevent the aggregation.

3.2. Ewald method: simple and lattice-based implementations

The famous Ewald method was invented at the beginning of the 20th century initially for computing conditionally converging lattice sums for the Coulomb interactions in ionic crystals and is now a standard method to calculate long-range interactions in systems with periodic boundary conditions. In such systems direct summation over all field sources (e.g., charges in Coulomb systems, dipoles in dipolar glasses, dislocations in crystal plasticity problems, etc) is obviously impossible due to their infinite number and we are forced to use the Fourier expansion over the reciprocal lattice vectors $\mathbf{k}$ corresponding to the infinitely repeated simulation cell. For *point* field sources the Fourier components of such an expansion decay relatively slowly (or may even not decay at all) with increasing magnitude of the wavevector k. By computer simulations we have at our disposal only a finite number of the wavevectors, so that we are forced to cut off the Fourier spectrum of our long-range interaction by some maximal and finite value $k_{\rm max}$. Due to the above-mentioned slow decay of the Fourier components these components at $k_{\rm max}$ are not small, so the spectrum cut-off is sharp and hence leads to large artificial oscillations of the interaction when transformed back to real space.

The Ewald method which we describe below for the specific case of a dipolar system cures the problem by *adding* and *subtracting* a Gaussian dipole at each point where initially a point dipole $\boldsymbol{\mu}_i$ is located, i.e., adding and subtracting a charge distribution

$$\rho_i^G(\mathbf{r}-\mathbf{r}_i) = -\frac{1}{(2\pi)^{3/2}\sigma^5}\cdot(\mathbf{r}-\mathbf{r}_i,\boldsymbol{\mu}_i)\cdot\exp\left(-\frac{(\mathbf{r}-\mathbf{r}_i)^2}{2\sigma^2}\right) \tag{3.2}$$

(this operation obviously does not change the resulting field). Then the total field $\mathbf{H}^{\rm dip}$ is calculated as the sum of the contributions $\mathbf{H}^{\rm dip} = \mathbf{H}^{\rm dip}_A + \mathbf{H}^{\rm dip}_{\rm B}$ of two subsystems: the first one consists of Gaussian dipoles (3.2) and the second one is composed from the original point dipoles minus the Gaussian dipoles (3.2):

$$\rho_{\rm B}(\mathbf{r}) = -\sum_i^N \left[\boldsymbol{\mu}_i \cdot \nabla\delta(\mathbf{r}-\mathbf{r}_i) - \rho_i^G(\mathbf{r}-\mathbf{r}_i)\right] \tag{3.3}$$

(the first term in square brackets represents the charge density corresponding to a point dipole at the location $\mathbf{r}_i$). The field created by a charge distribution in square brackets of (3.3) can be computed analytically ($\alpha = x, y, z$):

$$H^{\alpha}_{B,i}(\mathbf{r}-\mathbf{r}_i) = \left[\frac{3(\alpha-\alpha_i)(\boldsymbol{\mu}_i\Delta\mathbf{r}_i)}{(\Delta r_i)^5} - \frac{\mu_i^{\alpha}}{(\Delta r_i)^3}\right] f_G(\Delta r_i) + \sqrt{\frac{2}{\pi}}\frac{(\alpha-\alpha_i)(\boldsymbol{\mu}_i\Delta\mathbf{r}_i)}{(\Delta r_i)^5}\cdot\exp\left[-\frac{(\Delta r_i)^2}{2\sigma^2}\right] \tag{3.4}$$

where the function $f_G(r)$ decays exponentially with the distance:

$$f_G(r) = 1 - \mathrm{erf}\left(r/\sigma\sqrt{2}\right) + \sqrt{2/\pi}\cdot(r/a)\cdot\exp\left[-r^2/2\sigma^2\right]. \tag{3.5}$$

The decisive advantage of such a decomposition of the original point dipole system is the following. The field (3.4) from the second subsystem is a *short-range* one, because the initial point dipole is screened by a corresponding Gaussian dipole with the same total moment but having opposite sign. Hence this contribution can be calculated taking into account for each particle the fields from several nearest neighbours only and it takes for the whole system of N dipoles (particles) $\sim N$ operations. And the contribution from the first subsystem can be safely calculated by the Fourier expansion technique, because due to the *smooth* Gaussian charge distribution of the dipoles (3.2) their Fourier components decay rapidly with increasing k and hence no spurious oscillation arise due to the numerically unavoidable spectrum cut-off at large k. Details of this procedure can be found in Berkov and Gorn (1998).

Although the 'native' version of the Ewald method sketched above allows a reliable evaluation of the dipolar field for simulations with periodic boundary conditions, its important disadvantage for disordered systems is the high operation count ($\sim N^2$). The reason is that in such systems the particle positions do not form a regular and translationally invariant lattice, so that the Fourier expansion necessary to evaluate the long-range contribution from the Gaussian dipoles (subsystem A) cannot be evaluated using the *fast* Fourier transformation (FFT) technique: exponential factors $\exp(\mathrm{i}\mathbf{k}\mathbf{r}_i)$ should be computed for all wavevectors $\mathbf{k}$ and all particle positions $\mathbf{r}_i$ separately, leading to the operation count given above.

For this reason several lattice versions of the Ewald method have been developed (see the corresponding overview, e.g., in Deserno and Holm (1998)), where various mappings of the initial disordered system onto a regular lattice are used to enable the application of the FFT for the computation of the long-range contribution from the system of Gaussian dipoles. Lacking the space for the comparative analysis of all these versions, we would like to justify our choice of the following algorithm.

(i) First we map the disordered system of point (spherical) dipoles at locations $\mathbf{r}_i$ onto the system of magnetic moments located on the lattice points $\mathbf{r}_\mathbf{p}$ ($\mathbf{p}$ is the 3D-index) using some three-dimensional weighting function $w_{3\rm d}(\mathbf{r}_i - \mathbf{r}_\mathbf{p})$:

$$\tilde{\boldsymbol{\mu}}(\mathbf{r}_\mathbf{p}) = \sum_{i=1}^{N}\boldsymbol{\mu}(\mathbf{r}_i)w_{3\rm d}\left(|\mathbf{r}_i - \mathbf{r}_{\rm p}|\right) = \sum_{i=1}^{M_{\rm nb}}\boldsymbol{\mu}_i\cdot w\left(|x_i - x_{\rm p}|\right) w\left(|y_i - y_{\rm p}|\right) w\left(|z_i - z_{\rm p}|\right) \tag{3.6}$$

where we have assumed the $w(\mathbf{r})$ can be written as the product of factors depending on the coordinate differences along a single axis only. The whole method makes sense only if the function w can be chosen to be strongly localized (see below), so that the sum over formally all N particles in (3.6) is actually restricted to a few particles M_{nb} located near the lattice node $\mathbf{p}$.

(ii) At the second step we add and subtract to each point *lattice* dipole the two corresponding Gaussian dipoles in the form (3.2), as in the 'native' Ewald method.

(iii) Next we compute the dipolar field of this obtained system as described above, i.e., as the sum of the long-range contribution from the Gaussian dipoles *located on the lattice* and the short-range contribution (3.4) from the composite objects 'point dipole–Gaussian dipole' which are also placed on the lattice.

(iv) The last step is the mapping of the obtained field on *lattice* points $\mathbf{r_p}$ onto *initial* dipole locations $\mathbf{r}_i$ (using the same functions $w(x)$ as in (3.6)).

The advantage of this straightforward version of the lattice Ewald method is not only the possibility to use FFTs for computing the long-range part of the total dipolar field. Noting that (a) the short-range contribution (3.4) depends only on the *difference* $\Delta\mathbf{r}$ between the source and target coordinates and (b) both source and target points are located on the lattice, we can compute the short-range contribution as a discrete convolution also by the FFT technique. This allows us to increase the number of nearest number shells included into the evaluation of the short-range interaction part without additional time cost, so that the error associated with the truncation of the short-range interaction part can be made arbitrarily small. Taking into account that the evaluation of the long-range part via FFT for the *lattice* system is exact (there is no error due to the cut-off at the maximal wavevector k present for a disordered system), we conclude that the only error source for the algorithm described above is the mapping of the initial disordered system onto a lattice, which can be easily controlled and reduced by choosing the mapping scheme of a sufficiently high order (Deserno and Holm 1998). We have found that the conventional second-order mapping using the function

$$w(x) = \begin{cases} 3/4 - x^2, & 0 \leqslant |x| < 1/2 \\ (3/2 - |x|)^2/2, & 1/2 \leqslant |x| < 3/2 \end{cases} \tag{3.7}$$

(and $w = 0$ for $|x| > 3/2$) and the cubic lattice with the mesh size $\Delta x = R_{\mathrm{part}}$ gives by the evaluation of the dipolar field the relative error $\sim 10^{-4}$, which turned out to be small enough for all physical applications we have studied (see section 5).

3.3. Adaptation of the fast multipole method for the dipolar interaction

The fast multipole method (FMM) with its optimal operation count ($\sim N$) has been proved to be very useful by simulation of systems with gravitational and electrostatic interactions. By simulations of dipolar systems, however, this method has been barely used probably due to the following two reasons. First, the standard FMM (Greengard 1988) is based on the well-known series expansion of the function $1/r$ and so can be readily applied to the evaluation of electrostatic or gravitational potentials. The dipolar potential decays as $\sim 1/r^2$, making the analytical derivation of its multipole expansion not straightforward. The only attempt to use the FMM for dipolar systems was made by Kutteh *et al* (see, e.g., Kutteh and Nicolas 1995), where a few first multipole expansion coefficients for dipolar systems were calculated *manually* (in Cartesian coordinates), which obviously imposes a strong limitations on the expansion order and limits the simulation accuracy. Second, the lattice version (Deserno and Holm 1998) of the Ewald method for the simulation of dipolar systems (Wang and Holm 2001) can be developed

whose relatively straightforward implementation and favourable operation count $\sim N \log N$ makes it a powerful competitor to the FMM.

In this section we derive the analytical expression of multipole coefficients for the dipolar potential which can be directly applied to the calculations of magnetodipolar fields and forces in ferrofluids (our short note (Gorn and Berkov 2004) contains only the final result of this analysis) and compare afterwards the computational costs of the FMM and Ewald methods. We show that by the optimal choice of the hierarchical structure for the FMM method and the mapping procedure for the particle-mesh Ewald algorithm these methods demonstrate comparable performance for systems containing up to $\sim 4 \times 10^4$ particles.

To derive the analytical expression for multipole coefficients of a dipolar potential, we first recall that the Coulomb potential of a system of N charges q_i $(i = 1 \dots N)$ located at points $Q_i = (\rho_i, \alpha_i, \beta_i)$ can be evaluated at the target point $P = (r, \theta, \varphi)$, $r > \rho_i$, using the well-known series expansion $1/r_i' = \sum_{n=0}^{\infty} (\rho_i^n / r^{n+1}) \cdot P_n(\cos\gamma_i)$ (here $\mathbf{r}_i' = \mathbf{r} - \boldsymbol{\rho}_i$, $\gamma_i = \widehat{\boldsymbol{\rho}}_i$, $\mathbf{r}$ and P_n are Legendre polynomials). The resulting expansion of the Coulomb potential is:

$$\Phi(P) = \sum_{i=1}^{N} q_i \sum_{n=0}^{\infty} \frac{\rho_i^n}{r^{n+1}} P_n(\cos\gamma_i) = \sum_{n=0}^{\infty} \sum_{k=-n}^{n} M_n^k \frac{Y_n^k(\theta, \phi)}{r^{n+1}},$$

where $M_n^k = \sum_{i=1}^{N} q_i \rho_i^n Y_n^{-k}(\alpha_i, \beta_i)$ are multipole coefficients and Y_n^k denote spherical functions. The FMM uses these coefficients for calculation of a far-field contribution to the potential (the near-field part is evaluated by direct summation). Our aim is to evaluate these coefficients for a system of *dipoles*. Afterwards they can be used in the dipolar FMM version in the same way as in electrostatics.

We consider now a system of N dipoles $\boldsymbol{\mu}_i$ located at points $Q_i = (\rho_i, \alpha_i, \beta_i)$. We build each dipole $\boldsymbol{\mu}_i$ as a limiting case of the following standard construction: a pair of charges $q_i^+ = q_i$ and $q_i^- = -q_i$ are located at points $Q_i^+ = (\rho_i^+, \alpha_i^+, \beta_i^+)$ and $Q_i^- = (\rho_i^-, \alpha_i^-, \beta_i^-)$ connected via the vector $2\mathbf{d}_i$ (so that $\boldsymbol{\rho}_i^+ = \boldsymbol{\rho}_i + \mathbf{d}_i$ and $\boldsymbol{\rho}_i^- = \boldsymbol{\rho}_i - \mathbf{d}_i$). The length $d_i \to 0$ and the charge magnitudes $q_i \to \infty$ so that the product $2\mathbf{d}_i q_i = \boldsymbol{\mu}_i$ remains constant. For each pair of charges we write the potential in the same way as for the electrostatic case using the multipole coefficients:

$$M_{n,i}^k = \lim_{2\mathbf{d}_i q_i \to \boldsymbol{\mu}_i} q_i \cdot [(\rho_i^+)^n Y_n^{-k}(\alpha_i^+, \beta_i^+) - (\rho_i^-)^n Y_n^{-k}(\alpha_i^-, \beta_i^-)].$$

Next we expand the expressions for ρ_i^+ and ρ_i^- at the points Q_i^+ and Q_i^- over the magnitude d_i of the (small) vector $\mathbf{d}_i$ as (here and below $\tilde{d}_i = d_i/\rho_i$):

$$\begin{aligned}(\rho_i^{\pm})^n &= (\rho_i^2 \pm 2\rho_i d_i \cos\psi_i + d_i^2)^{n/2} = \rho_i^n \left(1 \pm 2\tilde{d}_i \cos\psi_i + o(\tilde{d}_i)\right)^{n/2} \\ &\approx \rho_i^n \left(1 \pm n \cdot \tilde{d}_i \cos\psi_i\right),\end{aligned}$$

(ψ_i is the angle between $\boldsymbol{\rho}_i$ and $\mathbf{d}_i$) and expressions for Y_n^{-k} over Cartesian coordinates of $\mathbf{d}_i$ (taking into account that $\partial Y_n^k / \partial r = 0$) as

$$\begin{aligned}Y_n^{-k}(\alpha_i^{\pm}, \beta_i^{\pm}) &\triangleq Y_n^{-k}(\boldsymbol{\rho}_i \pm \mathbf{d}_i) = Y_n^{-k}(\boldsymbol{\rho}_i) \pm (\mathbf{d}_i, \nabla) \cdot Y_n^{-k}(\boldsymbol{\rho}_i) + o(\mathbf{d}_i) \\ &\simeq Y_n^{-k}(\alpha_i, \beta_i) \pm \left(\frac{d_{i,\alpha}}{\rho_i} \frac{\partial Y_n^{-k}(\alpha_i, \beta_i)}{\partial \alpha} + \frac{d_{i,\beta}}{\rho_i \sin\alpha} \frac{\partial Y_n^{-k}(\alpha_i, \beta_i)}{\partial \beta}\right).\end{aligned}$$

Next we transform the spherical coordinates of $\mathbf{d}_i$ to its Cartesian coordinates using standard transition formulae ($d_\alpha = d_x \cos\alpha \cos\beta + d_y \cos\alpha \sin\beta - d_z \sin\alpha$, $d_\beta = -d_x \sin\beta + d_y \cos\beta$) and after reordering of terms obtain the desired expression

$$Y_n^{-k}(\alpha_i^{\pm}, \beta_i^{\pm}) \simeq Y_n^{-k}(\alpha_i, \beta_i) \pm \frac{1}{\rho_i} \left(d_{i,x} H_{i,x,n}^{-k} + d_{i,y} H_{i,y,n}^{-k} + d_{i,z} H_{i,z,n}^{-k}\right),$$

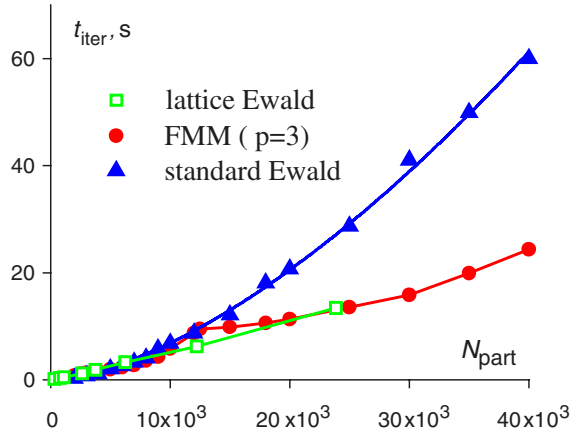

Figure 2. Performance comparison of various methods used to calculate the dipolar field in systems with periodic boundary conditions (see text for details).

(This figure is in colour only in the electronic version)

with the vector

$$\mathbf{H}_{i,n}^{k} = \frac{1}{\sin\alpha_i}\begin{pmatrix} \cos\alpha_i \sin\alpha_i \cos\beta_i \cdot \partial_\alpha Y_n^k(\alpha_i,\beta_i) - \sin\beta_i \cdot \partial_\beta Y_n^k(\alpha_i,\beta_i) \\ \cos\alpha_i \sin\alpha_i \sin\beta_i \cdot \partial_\alpha Y_n^k(\alpha_i,\beta_i) + \cos\beta_i \cdot \partial_\beta Y_n^k(\alpha_i,\beta_i) \\ -\sin^2\alpha_i \cdot \partial_\alpha Y_n^k(\alpha_i,\beta_i) \end{pmatrix}.$$

(here $\partial_\alpha \equiv \partial/\partial\alpha$, etc). Substituting the expansions of $\rho_i^{\pm}$ and $Y_n^{-k}(\alpha_i^{\pm},\beta_i^{\pm})$ into the formula for the multipole coefficients and simplifying the notation as $Y_n^{-k}(\alpha_i,\beta_i) \equiv Y_{n,i}^{-k}$, we can continue the calculation chain as follows:

$$\begin{aligned} M_{n,i}^{k} &= \lim_{2\mathbf{d}_i q_i \to \boldsymbol{\mu}_i} \left\{ q_i \rho_i^n \left[\left(1 + n\tilde{d}_i \cos\psi_i\right)\left(Y_{n,i}^{-k} + \left(\tilde{\mathbf{d}}_i, \mathbf{H}_{i,n}^{-k}\right)\right) \right.\right. \\ &\quad \left.\left. - \left(1 - n\tilde{d}_i \cos\psi_i\right)\left(Y_{n,i}^{-k} - \left(\tilde{\mathbf{d}}_i, \mathbf{H}_{i,n}^{-k}\right)\right) \right] \right\} \\ &= \lim_{2\mathbf{d}_i q_i \to \boldsymbol{\mu}_i} \rho_i^{n-1} \left[2q_i d_i \cdot n \cos\psi_i \cdot Y_{n,i}^{-k} + \left(2q_i \mathbf{d}_i, \mathbf{H}_{i,n}^{-k}\right) \right] \\ &= n\rho_i^{n-2}(\boldsymbol{\mu}_i, \boldsymbol{\rho}_i) \cdot Y_{n,i}^{-k} + \rho_i^{n-1}(\boldsymbol{\mu}_i, \mathbf{H}_{i,n}^{-k}). \end{aligned}$$

After taking the sum over all N dipoles we obtain the final formula

$$M_n^k = \sum_{i=1}^{N} n \cdot \left(\boldsymbol{\mu}_i, \boldsymbol{\rho}_i\right) \cdot \rho_i^{n-2} Y_n^{-k}(\alpha_i,\beta_i) + \sum_{i=1}^{N} (\boldsymbol{\mu}_i, \mathbf{H}_{i,n}^{-k}) \cdot \rho_i^{n-1}.$$

3.4. Comparison of the method performances

In figure 2 we present the speed comparison of various methods discussed above plotting the time required for one evaluation of the magnetodipolar field on all particles as a function of the particle number. The absolute time values obviously depend on the specific computer architecture, but the relation of times for various methods was found to be almost computer independent as long as no parallel or multicore architecture was involved. All methods were adjusted to obtain the dipolar field with the same average relative accuracy $\approx 10^{-3}$. The adjustable parameters are: the number of wavevectors and the real space cut-off radius for the standard Ewald method, the number of multipole moments taken into account for the FMM and the lattice mesh size for the lattice version of the Ewald method.

It can be clearly seen that the 'normal' Ewald method (blue triangles), which has been accelerated by us in a standard way to obtain an operation count $\sim N^{3/2}$ (the blue line is the fit with the corresponding power law) becomes slower than both its competitors starting from the particle number $N_\mathrm{p} \sim 10^4$. We have strongly optimized the FMM by introducing additional storage for the intermediate results and then the FMM was found to be comparable with the FFT Ewald method already for the same moderate particle numbers $\sim 10^4$. We expect the FMM to become clearly superior for $N_\mathrm{p} \sim 3 \times 10^4$, where we could not test the lattice Ewald method due to a high amount of computer memory required to store information for all nodes of the large 3D lattice with mesh size comparable to the particle radius.

4. Hydrodynamic interaction

To introduce the analytical description of the hydrodynamic interaction, we use a simplified model of a ferrofluid, the rigid dipole model, and consider the case when all particles are equipped with magnetic moments of equal magnitude and immersed in an *incompressible* carrier liquid. On the pertinent slow timescales the dynamics of these ferroparticles can be viewed as a stochastic Wiener process.

We denote the position of particle n by $\mathbf{R}_n \in \mathbb{R}^3$, the orientation of its magnetic moment by $\mathbf{E}_n \in S^2$ (the unit sphere surface) and put $\mathbf{X}_n = (\mathbf{R}_n, \mathbf{E}_n)$. On the Brownian timescale, the probability density $P(\mathbf{X}, t)$ in the many-body configuration space, with $\mathbf{X} = (\mathbf{X}_1, \mathbf{X}_2, \ldots)$, is governed by the generalized Smoluchowski equation (Felderhof and Jones 1993)

$$\frac{\partial}{\partial t} P(\mathbf{X}, t) = \sum_{n,m} \frac{\partial}{\partial \mathbf{X}_n} \cdot \mathbf{D}_{nm}(\mathbf{X}) \cdot \mathrm{e}^{-\Phi(\mathbf{X})/kT} \frac{\partial}{\partial \mathbf{X}_m} \mathrm{e}^{\Phi(\mathbf{X})/kT} \cdot P(\mathbf{X}, t) \tag{4.1}$$

where the indices n, m label the particles. The potential $\Phi(\mathbf{X})$ involves magnetic interactions as well as steric repulsion, while the many-body hydrodynamic interaction enters via the diffusion tensor $\hat{\mathbf{D}}(\mathbf{X})$, which is related to the Stokesian mobility tensor $\hat{\mathrm{M}}(\mathbf{X})$ via the Einstein relation $\hat{\mathbf{D}}(\mathbf{X}) = k_\mathrm{B} T \hat{\mathrm{M}}(\mathbf{X})$.

Numerical simulations of the Wiener process are based on the stochastic Langevin equations (Kloeden and Platen 1995) associated with (4.1). In the Itô interpretation of the stochastic integral the position $\mathbf{X}(t)$ is updated according to

$$\mathbf{X}(t + \Delta t) = \mathbf{X}(t) + \mathbf{V}\left(\mathbf{X}(t)\right) \Delta t + \sqrt{k_\mathrm{B} T}\, \mathbf{g}\left(\mathbf{X}(t)\right) \cdot \mathbf{\Gamma} \sqrt{\Delta t} \tag{4.2}$$

where Δt is the time step, the drift velocity is given by

$$\mathbf{V}(\mathbf{X}) = -\hat{\mathrm{M}}(\mathbf{X}) \cdot \frac{\partial \Phi(\mathbf{X})}{\partial \mathbf{X}} - k_\mathrm{B} T \frac{\partial}{\partial \mathbf{X}} \cdot \hat{\mathrm{M}}(\mathbf{X}) \tag{4.3}$$

and $\mathbf{\Gamma}$ is a normalized Gaussian random force with zero mean and variance $\langle \mathbf{\Gamma}\mathbf{\Gamma} \rangle = 2 \cdot \hat{\mathbf{1}}$. The amplitude $\mathbf{g}(\mathbf{X})$ is defined by

$$\hat{\mathrm{M}}(\mathbf{X}) = g(\mathbf{X}) \cdot \mathbf{g}^\mathrm{T}(\mathbf{X}) \tag{4.4}$$

which amounts to a Cholesky decomposition of the symmetric positive-definite matrix $\hat{\mathrm{M}}(\mathbf{X})$. For numerical measurement of time-dependent correlation functions (corresponding to physical observables) we have to average over the stochastic paths. Numerically effective treatment of the hydrodynamic interaction requires fast algorithms for the computation of the mobility matrix $\hat{\mathrm{M}}(\mathbf{X})$ and its Cholesky decomposition (Banchio and Brady 2003).

We start with the computation of the mobility matrix for a given configuration $\mathbf{X}$ assuming periodic boundary conditions. The basic cell V, which is assumed to be a cube with the side L,

is decomposed into the fluid region V_0 and the particles B_n, $(n = 1, \ldots, N)$. The fluid obeys the quasistatic Stokes equations

$$\begin{aligned} \eta \Delta \mathbf{v} - \nabla p &= 0 \\ \nabla \cdot \mathbf{v} &= 0 \end{aligned} \qquad (\mathbf{x} \in V_0) \tag{4.5}$$

(here $\mathbf{v}(\mathbf{x})$ and $p(\mathbf{x})$ denote the flow velocity and pressure, while η is the shear viscosity). On the particle surfaces, ∂B_n, stick boundary conditions are applied

$$\mathbf{v} = \mathbf{U}_n + R_\mathrm{p} \boldsymbol{\Omega}_n \times \mathbf{n} \qquad (\mathbf{x} \in \partial B_n), \quad (n = 1, 2, \ldots) \tag{4.6}$$

where $\mathbf{U}_n$ and $\boldsymbol{\Omega}_n$ are the translational and angular velocities of particle n, respectively, while R_p is the particle radius and $\mathbf{n}$ the outer normal vector.

By applying Green's theorem, equation (4.5) can be transformed into the integral equation

$$\mathbf{v}(\mathbf{x}) = -\frac{1}{\eta} \left(\nabla\nabla - \Delta \hat{\mathbf{1}} \right) \sum_m \oint_{\partial B_m} \mathrm{d}S' \, G_2(\mathbf{x} - \mathbf{x}') \cdot \mathbf{f}_m(\mathbf{x}) \quad (\mathbf{x} \in V_0) \tag{4.7}$$

where $\mathbf{f}_m(\mathbf{x}) = \mathbf{n} \cdot \boldsymbol{\sigma}(\mathbf{x})$, with $\sigma = 2\eta \, (\nabla \mathbf{v})^S - p\hat{\mathbf{1}}$, is the force density exerted by the fluid on particle m. Moreover, $G_2(\mathbf{x})$ is the fundamental solution of the biharmonic problem

$$\begin{aligned} &\Delta\Delta G_2(\mathbf{x}) = \sum_{\boldsymbol{\lambda} \in \mathbb{Z}^3} \delta(\mathbf{x} - \mathbf{X}_{\boldsymbol{\lambda}}) - 1/L^3 \qquad (\mathbf{x} \in \mathbb{R}^3) \\ &\int_V \mathrm{d}V \, G_2(\mathbf{x}) = 0 \end{aligned} \tag{4.8}$$

where the sum runs over lattice $\mathbf{X}_{\boldsymbol{\lambda}} = L\boldsymbol{\lambda}$, $\boldsymbol{\lambda} \in \mathbb{Z}^3$. The explicit solution of (4.8) is

$$G_2(\mathbf{x}) = \frac{1}{L^3} \sum_{\boldsymbol{\lambda} \in \mathbb{Z}^3 \setminus \mathbf{0}} \frac{1}{K_{\boldsymbol{\lambda}}^4} \mathrm{e}^{\mathrm{i}\mathbf{K}_{\boldsymbol{\lambda}} \cdot \mathbf{x}} \tag{4.9}$$

with the sum running over the reciprocal lattice $\mathbf{K}_{\boldsymbol{\lambda}} = (2\pi/L) \cdot \boldsymbol{\lambda}$, $(\boldsymbol{\lambda} \in \mathbb{Z}^3)$ (Hasimoto 1959). Convergence of the sum (4.9) can be greatly improved by the Ewald method (Cichocki and Felderhof 1989).

To identify the mobility matrix $\hat{\mathrm{M}}(\mathbf{X})$ we first apply the boundary conditions (4.6), writing

$$\begin{aligned} \dot{\mathbf{R}}_n &= \mathbf{U}_n = \frac{1}{4\pi R_\mathrm{p}^2} \int_{\partial B_n} \mathrm{d}S \, \mathbf{v}(\mathbf{x}) \\ \dot{\mathbf{E}}_n &= -\mathbf{E}_n \times \boldsymbol{\Omega}_n = -\frac{3}{8\pi R_\mathrm{p}^3} \mathbf{E}_n \times \oint_{\partial B_n} \mathrm{d}S \, \mathbf{n} \times \mathbf{v}(\mathbf{x}) \end{aligned} \tag{4.10}$$

and insert (4.7) on the right-hand sides. This leads to a coupled set of integral equations for the surface force densities $\mathbf{f}_m(\mathbf{x})$, $(m = 1, \ldots, N)$, in terms of the particle velocities $(\dot{\mathbf{R}}_n, \dot{\mathbf{E}}_n)$, which can be solved approximately, e.g., by expansion in surface harmonics. Moreover, stationarity of the particle motion requires that the lowest-order moments of the force densities are balanced by the direct forces and torques,

$$\mathbf{F}_n = \oint_{\partial B_n} \mathrm{d}S \, \mathbf{f}_n(\mathbf{x}) = \frac{\partial \Phi}{\partial \mathbf{R}_n}, \qquad \mathbf{T}_n = R_\mathrm{p} \oint_{\partial B_n} \mathrm{d}S \, \mathbf{n} \times \mathbf{f}_n(\mathbf{x}) = \mathbf{E}_n \times \frac{\partial \Phi}{\partial \mathbf{E}_n}. \tag{4.11}$$

It follows that there are linear relations

$$\frac{\partial \Phi}{\partial \mathbf{R}_n} = -\sum_m \left[\boldsymbol{\varsigma}_{nm}^{\mathrm{TT}} \cdot \dot{\mathbf{R}}_n + \boldsymbol{\varsigma}_{nm}^{\mathrm{TR}} \cdot \dot{\mathbf{E}}_n \right], \qquad \frac{\partial \Phi}{\partial \mathbf{E}_n} = -\sum_m \left[\boldsymbol{\varsigma}_{nm}^{\mathrm{RT}} \cdot \dot{\mathbf{R}}_n + \boldsymbol{\varsigma}_{nm}^{\mathrm{RR}} \cdot \dot{\mathbf{E}}_n \right] \tag{4.12}$$

which involve a friction matrix $\hat{\boldsymbol{\zeta}}(\mathbf{X})$, and, upon inversion,

$$\begin{aligned}\dot{\mathbf{R}}_n &= -\sum_m \left[\mathrm{M}^{\mathrm{TT}}_{nm} \cdot \frac{\partial \Phi}{\partial \mathbf{R}_m} + \mathrm{M}^{\mathrm{TR}}_{nm} \cdot \frac{\partial \Phi}{\partial \mathbf{E}_m} \right] \\ \dot{\mathbf{E}}_n &= -\sum_m \left[\mathrm{M}^{\mathrm{RT}}_{nm} \cdot \frac{\partial \Phi}{\partial \mathbf{R}_m} + \mathrm{M}^{\mathrm{RR}}_{nm} \cdot \frac{\partial \Phi}{\partial \mathbf{E}_m} \right]\end{aligned} \tag{4.13}$$

where the mobility matrix is defined via $\hat{\mathrm{M}}(\mathbf{X}) = \hat{\zeta}^{-1}(\mathbf{X})$.

The crucial point of the calculation is, of course, the solution of the integral equations. In fact, these are integral equations of the first kind, and therefore numerically poorly conditioned. However, it is possible (Kim and Karrira 1991) to reformulate the problem in terms of integral equations of the second kind, which are much better conditioned. Also it is possible to calculate the mobility matrix directly, rather than via inversion of the friction matrix.

The lowest multipole approximation (the simplest within the above scheme) is given by

$$\mathbf{f}_n(\mathbf{x}) = \frac{1}{4\pi R_{\mathrm{p}}^2}\mathbf{F}_n - \frac{3}{8\pi R_{\mathrm{p}}^3}\mathbf{n} \times \mathbf{T}_n + \cdots = \frac{1}{4\pi R_{\mathrm{p}}^2}\frac{\partial \Phi}{\partial \mathbf{R}_n} - \frac{3}{8\pi R_{\mathrm{p}}^3}\mathbf{n} \times \left(\mathbf{E}_n \times \frac{\partial \Phi}{\partial \mathbf{E}_n} \right) + \cdots \tag{4.14}$$

which amounts to neglecting all multipole moments that are not compensated by the direct forces (resp. torques). Although this model is only of limited value as far as quantitative accuracy is concerned, it contains the basic physical features of the hydrodynamic interaction, in particular its long-range and multi-particle character.

Inserting (4.14) into (4.7) and proceeding as described above, one arrives at the following explicit expressions for the mobility matrix:

$$6\pi\eta R_{\mathrm{p}} \mathrm{M}^{\mathrm{TT}}_{nm}(\mathbf{X}) = \begin{cases} \left[-R_{\mathrm{p}} \oint_{\partial B_a(\mathbf{0})} \mathrm{d}S \, \Delta G_2(\mathbf{x}) + (2\pi/3)\tilde{R}^3 \right] \hat{\mathbf{1}} & (m = n) \\ \left[6\pi R_{\mathrm{p}} (\nabla\nabla - \Delta\hat{\mathbf{1}} + (R_{\mathrm{p}}^2/3)\nabla\nabla\Delta) G_2(\mathbf{R}_{nm}) + 2\pi \tilde{R}^3 \hat{\mathbf{1}} \right] & (m \neq n) \end{cases}$$

$$2\eta \cdot \mathrm{M}^{\mathrm{TR}}_{nm}(\mathbf{X}) = (\mathbf{E}_m \nabla - \mathbf{E}_m \cdot \nabla\hat{\mathbf{1}}) \Delta G_2(\mathbf{R}_{nm}) \qquad (m \neq n)$$

$$2\eta \cdot \mathrm{M}^{\mathrm{RT}}_{nm}(\mathbf{X}) = (\nabla\mathbf{E}_n - \mathbf{E}_n \cdot \nabla\hat{\mathbf{1}}) \Delta G_2(\mathbf{R}_{nm}) \qquad (m \neq n)$$

$$8\pi\eta R_{\mathrm{p}}^3 \mathrm{M}^{\mathrm{RR}}_{nm}(\mathbf{X}) = \begin{cases} [1 - (4\pi/3)\tilde{R}^3](\hat{\mathbf{1}} - \mathbf{E}_n\mathbf{E}_n) & (m = n) \\ \left[2\pi R_{\mathrm{p}}^3 (\mathbf{E}_n \times \nabla)(\mathbf{E}_m \times \nabla) \Delta G_2(\mathbf{R}_{nm}) \right. \\ \quad \left. + 2\pi \tilde{R}^3 (\mathbf{E}_m \cdot \mathbf{E}_n \hat{\mathbf{1}} - \mathbf{E}_m\mathbf{E}_n) \right] & (m \neq n) \end{cases}$$

where $\mathbf{R}_{nm} = (\mathbf{R}_n - \mathbf{R}_m) \bmod L$, $\tilde{R} = R_{\mathrm{p}}/L$ and the rotation-translational self-coupling is zero (matrix elements $\hat{\mathrm{M}}^{\mathrm{RT}}_{nn} = \hat{\mathrm{M}}^{\mathrm{TR}}_{nn} = 0$).

Efficient calculation of the mobility matrix $\hat{\mathrm{M}}$ is the subject of special research, the results of which will be reported elsewhere. In the physical examples shown below we did not take the hydrodynamic interaction into account.

5. Physical results

In this section we present several applications of the Langevin dynamics simulations for studies of various ferrofluid properties, comparing, where possible, the results for the rigid dipole model and the ferrofluid model with internal degrees of freedom.

5.1. Equilibrium magnetization of a ferrofluid

The equilibrium properties of any physical system, being time independent, are normally not a subject of the Langevin dynamics simulations, which are designed to study time-dependent phenomena. However, this does not mean that the equilibrium properties *cannot* be studied using Langevin dynamics: performing such simulations we can follow a system evolution during a sufficiently long time to arrive at its thermodynamically equilibrium state. Starting from this point, we can record any physical quantity of interest during the simulation run and measure the corresponding average. If the system is ergodic, this time-averaged value coincides with the corresponding ensemble-averaged value in the thermodynamically equilibrium state. Such measurements of equilibrium properties using Langevin dynamics obviously make sense only if the relaxation from the starting state to the equilibrium is so fast than it can be reached during a reasonable computation time.

The practically most relevant ferrofluid property which can be measured by Langevin dynamics simulations is its equilibrium magnetization as a function of temperature and external field $M(H, T)$. In particular, in the rigid dipole model, where Néel relaxation and hence the corresponding energy barriers are absent, the equilibration time has the same order of magnitude as the rotational Brownian motion time $\tau_B^{rot} = 3\eta V_p/kT$ of spheres with the hydrodynamic radius of typical ferrofluid particles. For most ferrofluids this time is in the μs range, making Langevin dynamics simulations meaningful. In many cases Langevin dynamics may be even more efficient than the analogous Monte Carlo simulations. The reason is that the stochastic integration time step does not depend on the system size, whereby the average particle displacements which can be performed during one MC step strongly decrease with growing system size (because by the random displacement of all particles energy fluctuations grow with the system size when the average particle displacement is kept constant).

Corresponding detailed studies of the equilibrium ferrofluid magnetization have been done in Wang *et al* (2002) within the rigid dipole model using the Langevin equations with the inertial terms included. Such an inclusion is not really necessary for an overwhelming majority of practically relevant cases, especially when the simulation goal is the study of the equilibrium properties, but the results obviously remain valid.

Here we would like only to demonstrate that inclusion of the magnetic degrees of freedom does not change the equilibrium ferrofluid magnetization, so that the results obtained within the rigid dipole and flexible moment models should coincide. To do this, we begin with the standard expression of the equilibrium ferrofluid magnetization, writing the average projection of the unit magnetization vector on the field direction as

$$\langle m_z(H, T)\rangle = \frac{1}{Z}\int \mathrm{d}\Omega_{\mathbf{m}} \int \mathrm{d}\Omega_{\mathbf{n}} \cdot m_z \cdot \exp\left\{-\frac{E(\mathbf{m}, \mathbf{n}, \mathbf{H})}{kT}\right\} \tag{5.1}$$

where for a *non-interacting* system the energy E depends only on the moment direction $\mathbf{m}$, direction of the particle anisotropy axis $\mathbf{n}$ and the external field $\mathbf{H}$

$$E = -\mu(\mathbf{m}, \mathbf{H}) + KV \sin^2 \psi_{\widehat{\mathbf{n},\mathbf{m}}} = -\mu \cos\theta_{\mathbf{m}} - KV(\mathbf{n}, \mathbf{m})^2, \tag{5.2}$$

and the statistical sum Z is represented by the same integral as written explicitly in (5.1), but without m_z in the integrand. By integration over the magnetic moment orientations $\Omega_{\mathbf{m}}$ spherical coordinate axes are fixed due to the presence of an external field and the term $(\mathbf{m}, \mathbf{H})$ in the energy (5.2). In contrast, the orientation of the spherical coordinate system used by the integration over the orientation of the anisotropy axis directions $\Omega_{\mathbf{n}}$ may be chosen arbitrary. If we choose the polar axis direction along the current direction of the moment the integral (5.1) can be written as the product of factors dependent either on the moment direction or on the orientation of the anisotropy axis with respect to the instantaneous moment orientation:

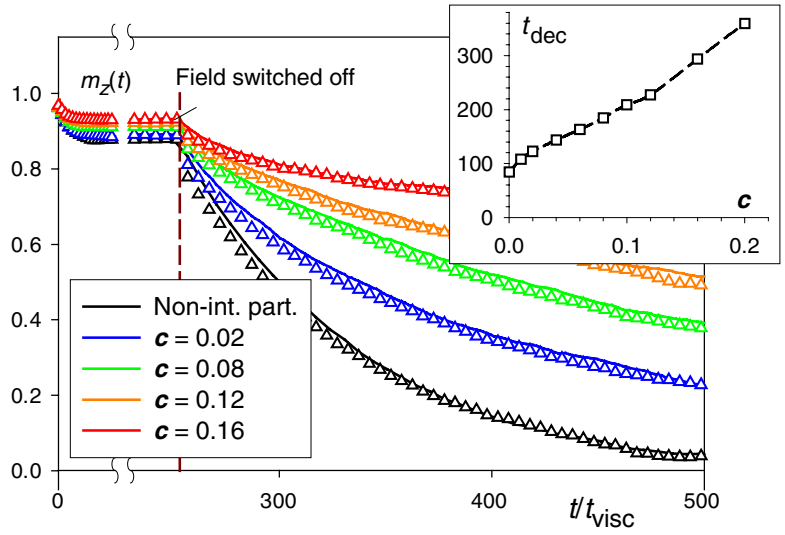

Figure 3. Magnetization relaxation after switching off the external field for ferrofluids with different particle concentrations (as shown in the legend). Particle parameters are $R_{mag} = 10$ nm, shell thickness $h = 2$ nm, magnetization $M_S = 400$ G. The solid lines are relaxation curves for the *rigid dipole* model, and open triangles stand for *'flexible' magnetic moments* with the reduced anisotropy constant $\boldsymbol{\beta} = \mathbf{2.0}$. The inset shows the dependence of the relaxation times (calculated from the initial curve slopes) on the particle concentration.

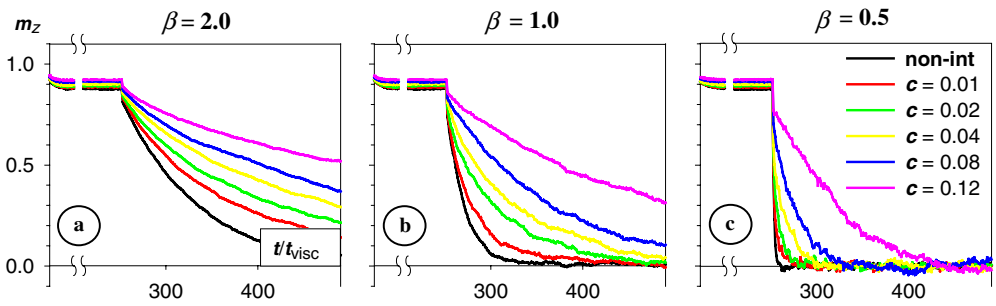

Figure 4. The same relaxation as shown in figure 3 for ferrofluids with 'flexible' magnetic moments and various single-particle anisotropy constants β as shown in the figure. It can be clearly seen that (i) already for the moderate anisotropy $\beta = 1.0$ the relaxation is much faster than for the rigid dipole model and (ii) the influence of the magnetodipolar interaction is much stronger for a system of particles with smaller anisotropy.

$$\langle m_z(H,T)\rangle = \frac{1}{Z_{\mathbf{m}} \times Z_{\mathbf{n}}} \int \mathrm{d}\Omega_{\mathbf{m}} \cdot m_z \cdot \exp\left\{\frac{\mu H \cos\theta_{\mathbf{m}}}{kT}\right\} \times \int \mathrm{d}\Omega_{\mathbf{n}} \cdot \exp\left\{-\frac{KV\cos^2\theta_{\mathbf{n}}}{kT}\right\}. \tag{5.1b}$$

The second factor cancels with the corresponding factor $Z_{\mathbf{n}}$ from the statistical sum Z (which can be factorized in the same way) and thus any information about the orientation of anisotropy axes, the value of the anisotropy constant, etc, disappears from the average magnetization. This proof can be easily generalized to the case of interacting particles, leading to the conclusion that including the internal magnetic degrees of freedom does not change the equilibrium magnetization properties of a ferrofluid.

5.2. Magnetic relaxation after switching off an external field

One of the processes widely used by ferrofluid applications is the relaxation of the ferrofluid magnetization after a ferrofluid is magnetized in an external field and this field is then switched off. The relaxation dynamics of the ferrofluid magnetization in such an experiment can be conveniently simulated using the Langevin dynamics, because the corresponding relaxation time is of the same order of magnitude as the rotational diffusion time $\tau_B^{rot} = 3\eta V_p/kT$ mentioned above. In this subsection we present example results of such simulations for a water-based ($\eta = 10^{-2}$ P) ferrofluid consisting of identical particles with the following parameters: magnetic kernel radius $R_{mag} = 10$ nm, shell thickness $h = 2$ nm, magnetization $M_S = 400$ G (magnetite). We study the effects of the anisotropy strength and magnetodipolar interparticle interaction, which can be controlled by the changing the particle volume fraction (concentration) c. All relaxation curves presented below were obtained by averaging over eight independent runs on systems containing $N_p = 1000$ particles each.

In figure 3 we compare the magnetization relaxation for the rigid dipole model and a ferrofluid with 'flexible' magnetic moments. For particles with the magnetic radius given above and a relatively large single-particle anisotropy $\beta = 2.0$ chosen for these simulations the relation of the anisotropy energy barrier to the thermal energy is high ($\beta M_S^2 V_{mag}/2kT \approx 16$). Hence we expect that the Néel relaxation can be neglected and the two models give equivalent results. This is indeed the case, as can be clearly seen by comparing the relaxation curves in figure 3 for one and the same concentration obtained from the rigid dipole model (solid lines) and ferrofluids with 'flexible' dipoles (open triangles). The only difference between the models is a slightly lower initial magnetization in the model with 'flexible' dipoles, which is due to the obvious reason that additional thermal fluctuations of magnetic moments around the anisotropy axis decrease the equilibrium magnetization.

However, already for the anisotropy $\beta = 1.0$ (only two times smaller than in previous simulations) the magnetization relaxation is substantially faster than for the rigid dipoles due to a significant contribution of the Néel relaxation: compare, for example, the black lines in figures 4(a) and (b) which show magnetization relaxation for systems of non-interacting particles with $\beta = 2.0$ and $\beta = 1.0$. For $\beta = 0.5$ the Néel relaxation is so fast that it is practically instantaneous on the timescale of the viscous Brownian motion (see the black line in figure 4(c)). This happens because although the relation of the anisotropy energy barrier to the thermal energy is still relatively large, $\beta M_S^2 V_{mag}/2kT \approx 4$, the prefactor before the exponent is so small that the corresponding transition time is much smaller then the Brownian time τ_B^{rot} (see the last row in table 1).

Another important effect clearly visible from our simulation results is a much stronger influence of the magnetodipolar interparticle interaction for systems with smaller anisotropy values. Whereas for $\beta = 2.0$ the decay time for the highest shown concentration ($c = 0.12$) is only about three times larger than for the non-interacting system (see inset to figure 3), for a system with $\beta = 0.5$ the relation of corresponding relaxation times exceeds $t^{dec}_{c=0.12}/t^{dec}_{non-int} > 10^3$. The reason for such an enhancement of the interaction influence is its qualitatively different role in ferrofluids consisting of particles with high and low anisotropy barriers. For particles with high anisotropy values the magnetodipolar interaction 'only' causes substantial magnetic moments correlations of neighbouring particles, thus increasing somewhat the corresponding relaxation time (such a 'dynamic' cluster relaxes slower than a single particle). In contrast to the previous situation, in systems with low-anisotropy particles the interaction field strongly increases the energy barriers for the Néel relaxation (Berkov 2002), thus leading to the exponential increase of the magnetization decay time.

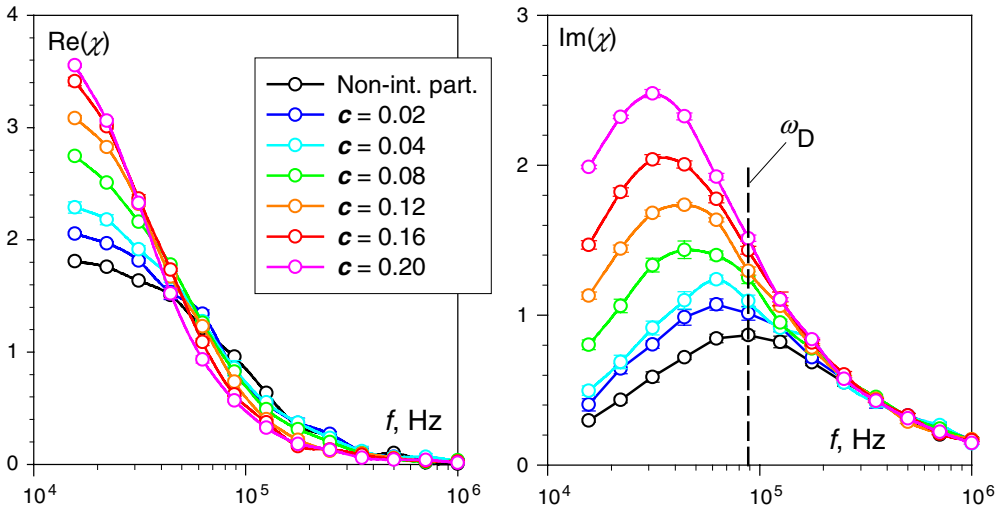

Figure 5. Frequency dependences of real and imaginary parts of the AC susceptibility $\chi(f, T)$ for ferrofluids with different particle concentrations (shown in the legend). Particle parameters are $R_{\mathrm{mag}} = 7$ nm, shell thickness $h = 1.5$ nm, magnetization $M_{\mathrm{S}} = 400$ G (*rigid dipoles* model).

5.3. AC susceptibility

Another important characteristic of a ferrofluid is its response to an alternating field, which for weak field amplitudes is characterized via its AC susceptibility $\chi(\omega)$ defined as the proportionality factor between the Fourier expansion coefficient $\mathbf{M}_\omega$ of the system magnetization $\mathbf{M}(t)$ and the corresponding Fourier coefficient $\mathbf{H}_\omega$ of the time-dependent external field $\mathbf{H}(t)$: $\mathbf{M}_\omega = \chi(\omega) \cdot \mathbf{H}_\omega$. Langevin dynamics provides the most straightforward way to compute the AC susceptibility by its definition, namely applying to the system a harmonic external field $\mathbf{H} = H_0 \mathbf{e}_z \cos(\omega t)$ of the given frequency along the z-axis and measuring the in-phase and out-of-phase response of the z-component of magnetization (L is the number of the time steps):

$$\begin{aligned} \mathrm{Re}(\chi) \equiv \chi' &= \frac{1}{H_0} \cdot \frac{1}{L} \sum_{l=1}^{L} \langle M_{l,z} \rangle \cdot \cos(\omega t_l), \\ \mathrm{Im}(\chi) \equiv \chi'' &= \frac{1}{H_0} \cdot \frac{1}{L} \sum_{l=1}^{L} \langle M_{l,z} \rangle \cdot \sin(\omega t_l). \end{aligned} \tag{5.3}$$

To obtain, for example, the frequency dependence of the AC susceptibility at a given temperature $\chi(\omega, T)$, one should repeat 'measurements' (5.3) at a set of frequencies sufficiently 'dense' to resolve all features of $\chi(\omega, T)$-dependence, which makes these simulations very time consuming. In principle, there exists an alternative way to compute the AC susceptibility: one can simulate the system response to a short and steep pulse of the external field. Such a pulse contains the contributions from all frequencies, so that a suitable transformation of the system response (magnetization time dependence $M(t)$) would provide at once the whole curve $\chi(\omega)$. Unfortunately, numerical Fourier transformation of noisy data is known as an ill-posed problem in the Hadamard sense (Press *et al* 1992), so that extremely high data accuracy (very small statistical error) is required to obtain reliable information concerning $\chi(\omega)$. For this reason, we have chosen the method (5.3), because it provides at least a possibility to estimate the measurements errors in a standard way and achieve reliable results in a reasonable computer time.

In figure 5 we plot $\chi(\omega, T)$ obtained within the *rigid dipoles* model at $T = 300$ K on a system of $N_p = 1000$ identical particles with the radii $R_{mag} = 7$ nm, shell thickness $h = 1.5$ nm and magnetization $M_S = 400$ G. Each point in figure 5 is the result of averaging (5.3) over at least four independent runs with duration $N_{cyc} = 5$ field cycles of the corresponding frequency. Again, the influence of the magnetodipolar interaction is of major interest. One can see that with the increasing interaction strength (increasing particle concentration) the real part of the susceptibility decreases for high frequencies and increases for low frequencies. At the same time the magnitude of the imaginary susceptibility part χ'' increases in the whole simulated frequency region, but this increase is much more strongly pronounced for lower frequencies. The peak in the $\chi''(\omega)$-dependence shifts to *lower* frequencies with increasing particle concentration, indicating the *increase* of the most probable relaxation time with the dipolar interaction strength (in a qualitative agreement with Zubarev and Yushkov (1998)). Such an increase of the relaxation time with the growing particle concentration was also observed in our simulations of the magnetization decay after switching off an external field. However, one should keep in mind that the magnetization decay in the latter case starts from the magnetization state which is qualitatively different from the nearly demagnetized state for which the linear AC susceptibility shown in figure 5 was 'measured', so that this similarity requires a special discussion.

Comparison of these results with simulation data obtained for a model with 'flexible' dipoles and with analytical theories will be presented elsewhere.

6. Conclusions and outlook

In this paper we have presented an overview of various numerical methods which should be used for Langevin dynamics simulations of ferrofluids for different relations between the characteristic system energies. Special attention in this discussion was paid to the fundamental difference between the rigid dipole model of a ferrofluid and a model in which magnetic degrees of freedom (rotation of a magnetic moment with respect to a particle itself) are included. We have also presented a variety of methods for the calculation of the magnetodipolar interaction and an analytical formalism for the treatment of the hydrodynamic interparticle interaction in the lowest multipole approximation. Finally we have shown several physical examples demonstrating the great potential of the Langevin dynamics by studies of the fast remagnetization processes in ferrofluids.

Further methodical effort should be undertaken towards the development of efficient numerical methods, especially for treating hydrodynamic interaction beyond the lowest multipole approximation (valid only in the small concentrations limit). Next, potential applications require simulations of *aggregated* ferrofluid: most ferrofluids have a substantial fraction of aggregates in their composition. Finally we note that meaningful comparison between simulations and experimental data will be possible only for carefully characterized ferrofluids, for which all basic particle parameters are known from independent measurements.

Acknowledgments

We thank the *Deutsche Forschungsgemeinschaft (DFG)* for the financial support of this research in frames of the German priority program SPP 1104 'Kolloidal magnetic fluids' (projects Be 2464/1-1, 1-2 and 1-3).

Appendix. Convergence rate of the multipole expansion for the dipolar potential

Here we derive the convergence rate of the multipole expansion series. In electrostatics, taking p moments one achieves an accuracy of the order $(a/r)^{p+1}$, where a is the radius of the sphere

enclosing all N charges ($a < r$). Now we are going to derive the corresponding error for the dipolar potential. For this purpose we consider again the system of charge pairs as above and introduce the angles $\gamma_i = \widehat{\boldsymbol{\rho}_i, \mathbf{r}}$, $\gamma_i^{\pm} = \widehat{\boldsymbol{\rho}_i^{\pm}, \mathbf{r}}$ and $\varphi_i = \widehat{\mathbf{d}_i, \mathbf{r}}$. The accuracy ε (depending on the number of moments p in the truncated series) can be estimated by the sum ($u_i = \cos(\gamma_i)$):

$$\varepsilon = \left| \Phi(P) - \left(\sum_{i=1}^{N} q_i \sum_{n=0}^{p} \frac{(\rho_i^+)^n P(u_i^+) - (\rho_i^-)^n P(u_i^-)}{r^{n+1}} \right) \right|$$
$$\leqslant \sum_{i=1}^{N} \underbrace{\left| \sum_{n=p+1}^{\infty} \frac{q_i}{r^{n+1}} \left((\rho_i^+)^n P(u_i^+) - (\rho_i^-)^n P(u_i^-) \right) \right|}_{\triangleq \varepsilon_i}.$$

To estimate the residuals ε_i we need the asymptotics of $(\rho_i^{\pm})^n \simeq \rho_i^n (1 \pm n(d_i/\rho_i)\cos\psi_i)$ and of $P_n(u_i^{\pm})$ which can be obtained from the Taylor expansion $P_n(u_i^{\pm}) \simeq P_n(u_i) + P_n'(u_i) \cdot \Delta u_i^{\pm}$. The asymptotic expression for $\Delta u_i^{\pm}$ can be derived in the following way (below $\delta_i = d_i/r_i$):

$$\Delta u_i^{\pm} = \cos\gamma_i^{\pm} - \cos\gamma_i = \frac{(\boldsymbol{\rho}_i^{\pm}, \mathbf{r})}{\rho_i^{\pm} \cdot r} - u_i = \frac{(\boldsymbol{\rho}_i, \mathbf{r}) + (\mathbf{d}_i, \mathbf{r})}{\rho_i (1 - \delta_i \cos\psi_i) r} - u_i$$
$$= \frac{\rho_i r u_i \pm d_i r \cos\varphi_i}{\rho_i (1 - \delta_i \cos\psi_i) r} - u_i$$
$$= (u_i \pm \delta_i \cos\varphi_i)(1 \mp \delta_i \cos\varphi_i) - u_i \simeq \pm\delta_i(\cos\varphi_i - u_i \cos\psi_i)$$
$$\equiv \pm\delta_i \cdot C_{\varphi_i, \psi_i, u_i}.$$

Substituting this expression in the expansion of Legendre polynomials and denoting $L_n(u_i) \triangleq P_n'(u_i)$, we have $P_n(u_i^{\pm}) \simeq P_n(u_i) \pm \delta_i \cdot L_n(u_i) \cdot C_{\varphi_i, \psi_i, u_i}$. Finally we substitute the asymptotic expressions for $(\rho_i^{\pm})^n$ and $P_n(u_i^{\pm})$ into the formula for ε_i:

$$\varepsilon_i \simeq \left| \sum_{n=p+1}^{\infty} \frac{q_i \rho_i^n}{r^{n+1}} \left[(1 + n\delta_i \cos\psi_i)(P_n(u_i) + \delta_i L_n(u_i) C_{\varphi_i, \psi_i, u_i}) \right. \right.$$
$$\left. \left. - (1 - n\delta_i \cos\psi_i)(P_n(u_i) - \delta_i L_n(u_i) C_{\varphi_i, \psi_i, u_i}) \right] \right|$$
$$\simeq \sum_{n=p+1}^{\infty} \frac{2 q_i \rho_i^n}{r^{n+1}} \delta_i \left(n P_n(u_i) \cos\psi_i + L_n(u_i) C_{\varphi_i, \psi_i, u_i} \right).$$

Using the inequalities $|\cos\psi_i| \leqslant 1$, $\left|C_{\varphi_i, \psi_i, u_i}\right| \leqslant 2$, $|P_n(u_i)| \leqslant 1$, $|L_n(u_i)| \leqslant n(n+1)/2$ (proof of the last one is a good exercise in the theory of special functions), we proceed as follows:

$$\varepsilon_i \leqslant \left| \sum_{n=p+1}^{\infty} \frac{2 q_i \rho_i^n}{r^{n+1}} \cdot \frac{d_i}{\rho_i} \underbrace{(n + n(n+1))}_{n(n+2)} \right| = \frac{\mu_i}{\rho_i} \left(\frac{\rho_i}{r} \right)^{p+1} \left| \sum_{n=0}^{\infty} \frac{\rho_i^n}{r^{n+1}} (n + p + 1)(n + p + 3) \right|$$
$$= \frac{\mu_i}{\rho_i} \left(\frac{\rho_i}{r} \right)^{p+1} \left[\frac{1}{r} \sum_{n=0}^{\infty} n^2 \left(\frac{\rho_i}{r} \right)^n + \frac{(2p+4)}{r} \sum_{n=0}^{\infty} n \left(\frac{\rho_i}{r} \right)^n \right.$$
$$\left. + \frac{(p+1)(p+3)}{r} \sum_{n=0}^{\infty} \left(\frac{\rho_i}{r} \right)^n \right]$$
$$= \frac{\mu_i}{\rho_i} \left(\frac{\rho_i}{r} \right)^{p+1} \left[\frac{1}{r} \cdot \frac{(\rho_i/r)(1 + \rho_i/r)}{(1 - \rho_i/r)^3} + \frac{(2p+4)}{r} \cdot \frac{(\rho_i/r)}{(1 - \rho_i/r)^2} \right.$$

$$+\frac{(p+1)(p+3)}{r}\cdot\frac{1}{(1-\rho_i/r)}\Bigg]$$
$$=\mu_i\left(\frac{\rho_i}{r}\right)^{p+1}\left[\frac{\rho_i+r}{(r-\rho_i)^3}+\frac{2(p+2)}{(r-\rho_i)^2}+\frac{(p+1)(p+3)}{\rho_i\,(r-\rho_i)}\right]$$
$$\simeq C\left(\frac{\rho_i}{r}\right)^{p+1}p^2\leqslant C\left(\frac{a}{r}\right)^{p+1}p^2,$$

where a is the radius of the sphere enclosing all N dipoles. Hence the total error $\varepsilon\sim Cn\,(a/r)^{p+1}\,p^2$ is slightly worse than its counterpart from electrostatics.

References

Banchio A J and Brady J F 2003 Accelerated Stokesian dynamics: Brownian motion *J. Chem. Phys.* **118** 10323

Berkov D V 2002 Density of energy barriers in fine magnetic particle systems *IEEE Trans. Magn.* **38** 2637

Berkov D V and Gorn N L 1998 Quasistatic remagnetization processes in two-dimensional systems with random on-site anisotropy and dipolar interaction: numerical simulations *Phys. Rev.* B **57** 14332

Berkov D V and Gorn N L 2001 Susceptibility of the disordered fine magnetic particle system: the Langevin-dynamics study *J. Phys.: Condens. Matter* **13** 9369

Berkov D V, Gorn N L and Stock D 2003 Remagnetization processes in ferrofluids: numerical simulations using the Langevin dynamics *Magnetohydrodynamics* **39** 97

Brown W F Jr 1963 Thermal fluctuations of a single domain particle *Phys. Rev.* **130** 1677

Cichocki B and Felderhof B U 1989 Periodic fundamental solution of the linear Navier-Stokes equations *Physica* A **159** 19

Coffey W, Kalmykov Yu R and Waldron J T 1996 *The Langevin Equation* (Singapore: World Scientific)

Davis S W, McCausland W, McGahagan H C, Tanaka C T and Widom M 1999 Cluster-based Monte-Carlo simulations of ferrofluids *Phys. Rev.* E **59** 2424

Deserno M and Holm C 1998 How to mesh up Ewald sums. I. A theoretical and numerical comparison of various particle mesh routines *J. Chem. Phys.* **109** 7678

Felderhof B U and Jones J B 1993 Orientational relaxation in a colloidal suspension of spheres *Phys. Rev.* E **48** 1084

Gorn N L and Berkov D V 2004 Adaptation and performance of the fast multipole method for dipolar systems *J. Magn. Magn. Mater.* **272–276P1** 698

Greengard L 1988 *The Rapid Evaluation of Potential Fields in Particle Systems* (Cambridge: MIT Press)

Hasimoto H 1959 On the periodic fundamental solution of the Stokes equations and their application to viscous flow past a cubic array of spheres *J. Fluid Mech.* **5** 317

Hockney R W and Eastwood J W 1981 *Computer Simulation Using Particles* (New York: McGraw-Hill)

Hoenggi P, Talkner P and Borkovec M 1990 Reaction-rate theory: fifty years after Kramers *Rev. Mod. Phys.* **62** 251

Huang J P, Wang Z W and Holm C 2005 Computer simulations of the structure of colloidal ferrofluids *Phys. Rev.* E **71** 061203

Ilg P, Kröger M, Hess S and Zubarev A 2003 Dynamics of colloidal suspensions of ferromagnetic particles in plane Couette flow *Phys. Rev.* E **67** 061401

Jund P, Kim S G, Tomanek D and Hetherington J 1995 Stability and fragmentation of complex structures in ferrofluids *Phys. Rev. Lett.* **74** 3049

Kim S and Karrira S J 1991 *Microhydrodynamics: Principles and Selected Applications* (Boston: Butterworth-Heinemann)

Kloeden P E and Platen E 1995 *Numerical Solution of Stochastic Differential Equations* (Berlin: Springer)

Kutteh R and Nicolas J B 1995 Implementing the cell multipole method for dipolar and charged dipolar systems *Comput. Phys. Commun.* **86** 236

Press W H, Teukolsky S A, Vetterling W T and Flannery B P 1992 *Numerical Recipes in Fortran: The Art of Scientific Computing* (Cambridge: Cambridge University Press)

Wang Z and Holm C 2001 Estimate of the cutoff errors in the Ewald summation for dipolar systems *J. Chem. Phys.* **115** 6351

Wang Z, Holm C and Müller H W 2002 Molecular dynamics study on the equilibrium magnetization properties and structure of ferrofluids *Phys. Rev.* E **66** 021405

Zubarev A and Yushkov A V 1998 Dynamic properties of moderately concentrated magnetic fluids *J. Exp. Theor. Phys.* **87** 484